International
Progress Report

IPR-05-30

Äspö Hard Rock Laboratory

Prototype Repository

Acoustic emission and ultrasonic monitoring during the heating of deposition hole DA3545G01 in the Prototype Repository to March 2005

J.R. Haycox
W.S. Pettitt
Applied Seismology Consultants

December 2005

Svensk Kärnbränslehantering AB
Swedish Nuclear Fuel
and Waste Management Co
Box 5864
SE-102 40 Stockholm Sweden
Tel 08-459 84 00
+46 8 459 84 00
Fax 08-661 57 19
+46 8 661 57 19

Äspö Hard Rock
Laboratory

Report no.	No.
IPR-05-30	F63K
Author	Date
J.R. Haycox W.S. Pettitt	December 2005
Checked by	Date
Lars-Erik Johannesson R.P. Young	2006-04-24
Approved	Date
Anders Sjöland	2006-04-28

Äspö Hard Rock Laboratory

Prototype Repository

Acoustic emission and ultrasonic monitoring during the heating of deposition hole DA3545G01 in the Prototype Repository to March 2005

J.R. Haycox
W.S. Pettitt
Applied Seismology Consultants

December 2005

Keywords: Field test, Prototype Repository, Acoustic emission, Ultrasonic monitoring, P-wave velocity, S-wave velocity, Rock fractures, Rock properties

Report DLV-05-03

To

SKB

APPLIED SEISMOLOGY CONSULTANTS

Last Edited	26 april 2006
File name	SKBProtoHeating_29072005.doc
Last Printed	26 april 2006
Signature	

Executive summary

This report describes results from acoustic emission (AE) and ultrasonic monitoring around a canister deposition hole (DA3545G01) during the heating phase in the Prototype Repository Experiment at SKB's Hard Rock Laboratory (HRL), Sweden. This monitoring aims to examine changes in the rock mass caused by an experimental repository environment, in particular due to thermal stresses induced from canister heating and pore pressures induced from tunnel sealing.

Ultrasonic monitoring has been conducted in two periods between 20th March and 9th October 2003, and 29th September 2004 to 31st March 2005. Two different techniques have been used in this study to examine the rock mass. AE monitoring is a 'passive' technique similar to earthquake monitoring but on a much smaller distance scale (source dimensions of millimetres). Ultrasonic surveys are used to 'actively' examine changes in the material properties of the rock through changes in recorded signal amplitudes and velocity.

Measurements from temperature and pressure instruments located in and around the deposition hole provide an indication of the major environmental changes occurring during this period. In April 2003 temperature starts to increase after heaters are switched on. The rate of temperature increase is high over the first few months but reduces over time. By the end of the second monitoring period the maximum temperature measured on the deposition hole wall is 52.8°C. On 1st November 2004, drainage from the tunnel was closed resulting in a steady increase in total pressure (sum of bentonite swelling pressure and pore pressure) recorded in the tunnel backfill above the deposition hole. No increases in total pressure are observed for instruments on the side wall of the deposition hole until a rapid increase starting 4th December 2004. Results from the ultrasonic surveys are presented in two phases corresponding to the first 6-month period, when thermal gradients were at their highest, and then the last 6 months when temperatures have reached a more steady state, but there are rapid and significant temporal changes in pressure.

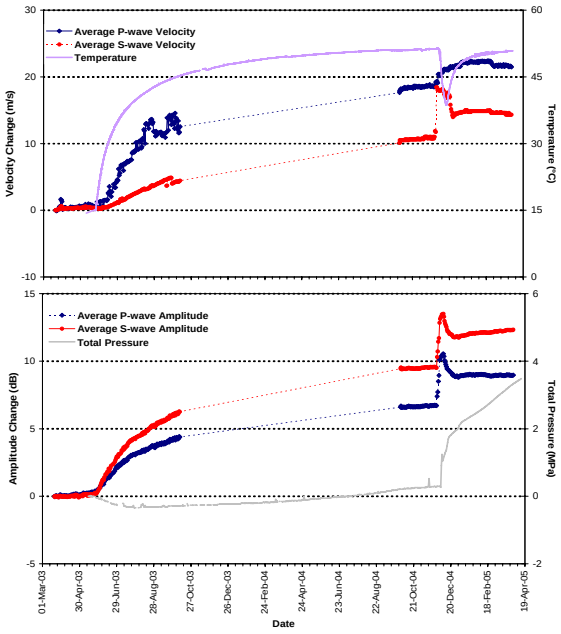

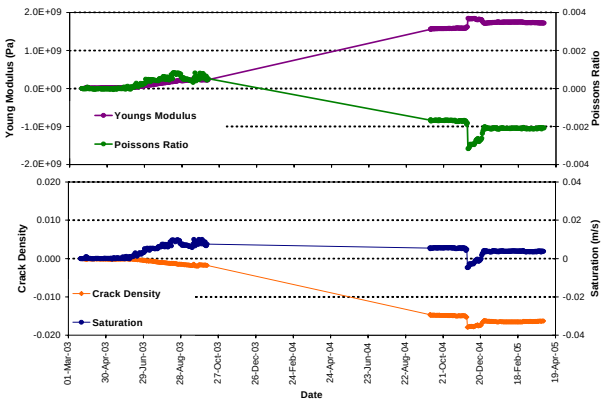

Average P- and S-wave velocity and amplitude change compared to pressure and temperature (left). Modulus changes for average values over the whole reporting period (right).

The majority of processed raypaths during the heating period show consistent behaviour, with the general trend being an increase in signal velocities and amplitudes for both P- and S-waves. Young's Modulus, Poisson's Ratio, Crack Density and Saturation parameters have been determined from the P- and S-wave velocities. An increase in Young's Modulus occurs during the heating period (indicating the rock gets gradually stiffer) and Crack Density reduces as cracks close. The increase in observed velocity and amplitude values is therefore due to closure of microcracks and pore spaces in the excavation damaged zone and surrounding stress-disturbed volumes indicating that thermal stresses are acting to increase the compressive stresses around the deposition hole. When unconfined rock samples are heated in a laboratory environment thermal expansion of the sample causes tensile stresses leading to an opening of existing microcracks. In the case of the Prototype Repository, the rock around the deposition hole is confined by the *in situ* stresses and the bentonite buffer. Expansion of the rock fabric cannot therefore act outwards and leads to compressive stresses acting on the existing microfractures and pore spaces.

The ultrasonic array geometry has been designed with 'skimming' raypaths that pass within a few centimetres of the deposition-hole void so as to sample the rock immediately adjacent to the deposition-hole wall. The ultrasonic measurements show that the low-compressive stress, or tensile, region induced by the *in situ* stress field around the excavation void is more responsive to heating, exhibiting rapid increases in P- and S-wave velocity. The high-compressive zone responds similarly over the whole monitoring period, exhibiting increases in velocity, but both P and S-wave velocities respond slower in the first few months of heating. The difference in the rate of response between the two raypath categories is interpreted as a different magnitude of response of the microfractures in the rock mass to increasing thermal stresses. In the low-compressive region, existing microfractures will initially be unloaded and hence more open than similar microfractures in the compressive region, where stresses act to clamp the fractures. As thermal stresses are applied to the rock mass the open fractures will be more sensitive to the stress increase and hence respond to a greater extent, and far quicker, than those that are pre-clamped, resulting in more responsive ultrasonic signals. The compressive stresses will be variable with orientation and hence may explain small differences recorded on individual ray paths.

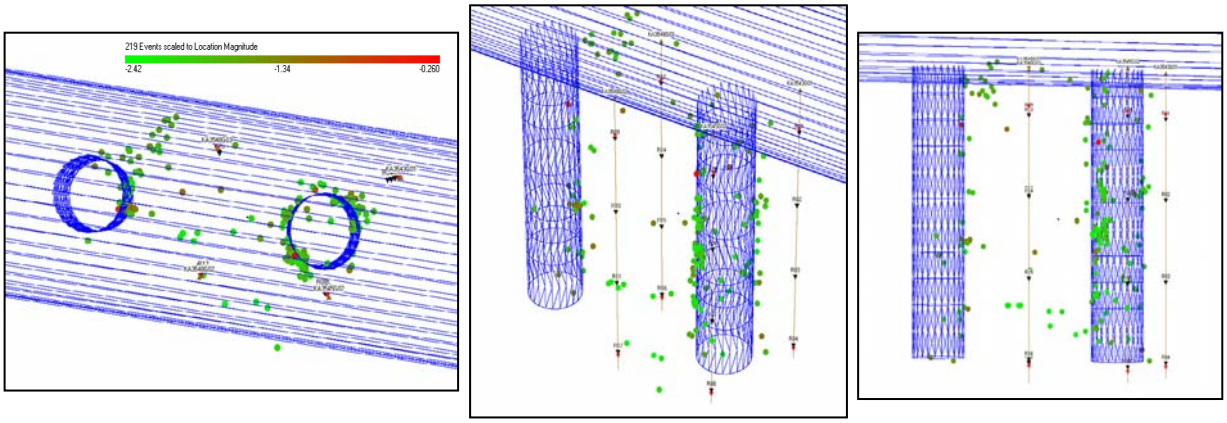

Projections of all AEs located during this reporting period. Events are scaled to instrument magnitude.

Another effect is superimposed onto the rock's response to thermal stresses. This is measured as a reduction in P-wave velocities compared to S-wave velocities in the first few months of heating. 'Saturation' values calculated from the measured P- and S-wave velocities show that a de-saturation occurs on all raypath categories during the first few months of monitoring, except for ray paths that pass through the low-compressive, or tensile, region. This must be caused by a drying of the rock mass as heat is applied to the rock (both pressure and temperature are acting to expel moisture). In the low-compressive, or tensile, region saturation increases during this period. This is probably caused by hot fluids expanding into the open microfracture fabric.

The increase in pressure induced in the Prototype at the end of November 2004 resulted in significant changes to the character of many recorded waveforms from the ultrasonic surveys. This suggests that as pressure is increased in the rock surrounding the deposition hole, attenuation of the ultrasonic waves is reduced meaning that they can pass more efficiently through the rock medium. The reduction in attenuation is either a result of an increase in saturation in the rock mass (fluids are pushed into microcracks and pore spaces), or a result of a reduction in crack density caused by a closing of pre-existing microcracks, or a combination of the two.

Significantly, velocity and amplitude changes recorded on the ultrasonic surveys occurred up to 10 days *before* the pressure change is recorded inside the deposition hole. A correlation is observed between the date on which the rapid changes in velocity and amplitude occur and the distance of the ray paths away from the tunnel, further down the deposition hole. The changes are observed between 26th November and 1st December and on all ray path categories irrespective of how close they pass the deposition hole void. This pattern does not appear in the pressure measurements recorded within the deposition hole on 4th-5th December. The modulus results show that the rock around the deposition hole generally stiffens and the crack density reduces. Our interpretation of these results is that a pressure and/or fluid field migrated through the rock mass at this time, initiated by pressure within the tunnel reaching a critical value on 26th November (approximately 0.75MPa). A fluid 'front' may have used the existing macro-fracture network to propagate away from the tunnel. The pressure or fluid field reached the floor level of the deposition hole on 1st December, but did not ingress into the deposition hole until 4th-5th December when a relatively sudden event occurred; it may have been inhibited by the bentonite buffer material. The event may have been induced by a combination of the pressure increases around the deposition hole and a rapidly cooling canister (the heaters were switched off on 2nd December).

Processing of acoustic emissions (AEs) has resulted in 219 events located with high confidence during the whole reporting period. The majority of the events locate close to the deposition hole wall, within the first 20cm and are distributed in the NE and SW quadrants that coincide with regions of increased compressive stress induced by the interaction of the stress field with the excavation void. This activity is interpreted as stress disturbance of the rock mass, particularly around pre-existing macrofractures that commonly intersect the excavation, or microcracking in the immediate vicinity of the fractures. 5% of the AEs locate within the pillar volume and define an approximately horizontal planar feature which coincides with a semi-horizontal macroscopic fracture that is observed to intersect the deposition holes at this height.

The peak rate of observed AE activity coincides with the rapid changes in pressure in the Prototype. A peak of 32 events occurs on 5th December 2005, when pressure in the buffer is highest, predominantly locating around deposition hole DA3545G01. The increase in activity is therefore likely to be the result of stress changes in the rock around the deposition hole associated with this relatively sudden increase in pressure. The stress changes are inducing small scale movements on pre-existing microfractures created during excavation, or are inducing new microfractures in weaker volumes of the rock. Pore pressure increases may also assist in inducing slip on pre-existing microfractures, by reducing the normal stress on the fractures.

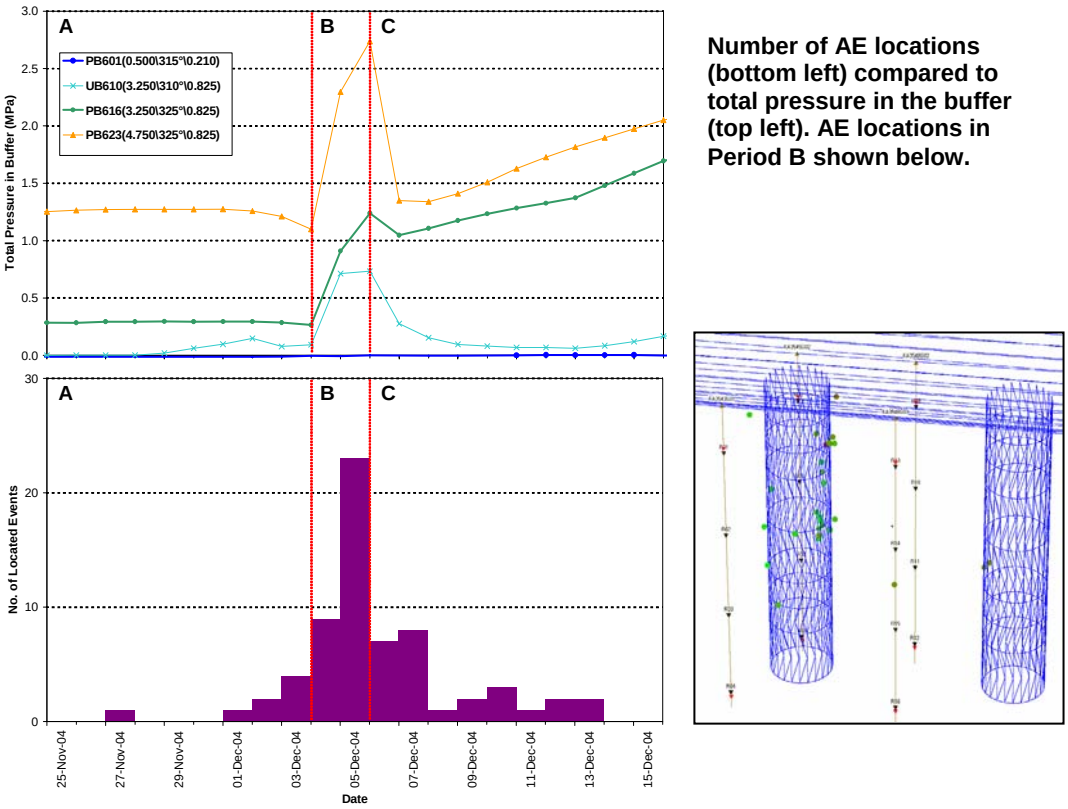

Number of AE locations (bottom left) compared to total pressure in the buffer (top left). AE locations in Period B shown below.

The overall AE activity rate is low compared to excavation, which indicates that heating of the deposition hole canisters has not so far resulted in a significant creation of new micro-fractures or the disturbance of pre-existing fractures. It is concluded that the thermal-related activity is a re-initiation of the same stress-related processes that occurred during excavation, although with a much reduced intensity. The AE activity did not start immediately heating began suggesting that the thermal stresses had to reach a certain level before AEs were triggered. This is likely to be the result of the Kaiser effect (well documented in laboratory experiments) where the AE rate is zero, or close to the background level, so long as stress remains below the largest previously reached stress value. In this case the largest stress value is that induced immediately behind the advancing face of the deposition hole during its excavation. The monitoring has shown that the rock is sensitive to sudden changes in conditions in the deposition-hole environment, such as the increase in pore pressure when drainage from the tunnel was closed off. This change in environmental conditions created a disturbance in the stress field around the deposition hole that was detected in both the ultrasonic survey and AE results.

Contents

Table of figures

Table of tables

1 Introduction

This report describes results from acoustic emission (AE) and ultrasonic monitoring around a canister deposition hole (DA3545G01) during the heating phase in the Prototype Repository Experiment at SKB's Hard Rock Laboratory (HRL), Sweden. This monitoring aims to examine changes in the rock mass caused by an experimental repository environment, in particular due to thermal stresses induced from canister heating and pore pressures induced from tunnel sealing. Monitoring was previously performed during excavation of the same canister deposition hole [*Pettitt et al.*, 1999a] and showed the mechanical response of the rock to induced excavation stresses.

The Prototype Repository Experiment (Figure 1-1) has been designed to simulate a disposal tunnel in a real deep repository for disposal of high-level nuclear waste. Its objective is 'to test and demonstrate the integrated function of the repository components under realistic conditions on a full scale and to compare results with models and assumptions'. The experiment consists of a 90m long, 5m diameter sub-horizontal tunnel excavated in a dioritic granite using a Tunnel Boring Machine (TBM). The rock mass has two main discontinuous sets of sparse, en-echelon fractures [*Patel et al.*, 1997]. The Prototype Repository design incorporates six full-scale canister deposition holes which have been excavated vertically into the floor of the tunnel using a TBM converted to vertical boring. Each deposition hole measures 1.75m in diameter and approximately 8.8m in length. Simulated waste canisters, encased in a bentonite buffer, have been placed into each deposition hole and heated from within by specially designed electric heaters to simulate disposed nuclear material. The tunnel was then backfilled using a mixture of bentonite and crushed rock, and sealed using concrete plugs.

AE and ultrasonic monitoring is one of a number of scientific measurements being used to remotely monitor the performance of the Prototype Repository. *Goudarzi and Johannesson*[2004] presents the locations and results from temperature, total-pressure, pore water pressure and water saturation instruments. These measurements are used in this report to assist in the interpretation of the ultrasonic results. In particular, temperature and total pressure measured on the rock wall of the deposition hole (Figure 1-2) are related to significant changes that are observed in the ultrasonic measurements.

AE and ultrasonic monitoring is a tool for examining the extent and severity of damage and disturbance around an excavation. This can be induced by the excavation method itself, by the redistribution of stresses (loading or unloading) resulting from the void or by environmental effects such as heating, saturation or pressurisation. The spatial extent, temporal dependence and scale of fracturing and the effect of this on the overall stability of the rock mass, is of high interest to engineers particularly when the integrity of a structure is critical to the performance of a project. Acoustic techniques are particularly adept at assessing the Excavation Damaged or Disturbed Zone (EDZ) as they allow it to be mapped spatially and temporally with high resolution, and they allow the effect on the rock mass to be quantifiably measured. Furthermore, acoustic techniques allow investigations to be conducted remotely, without the need for potentially damaging coring. *Young and Pettitt* [2000] give a review of AE and ultrasonic results from a number of experiments conducted in different underground environments.

Two techniques have been utilised during the monitoring to investigate the processes occurring within the rock mass around the deposition hole:

- AE monitoring is a 'passive' technique similar to earthquake monitoring but on a much smaller distance scale (source dimensions of millimetres). AEs occur on fractures in the rock sample when they are created or when they move. The data acquisition system triggers on AEs when they occur and records full-waveform information that can then be used to delineate the amount, time, location and mechanism of fracturing.
- Ultrasonic surveys are used to 'actively' examine the rock. In this case an array of transmitters sends signals to an array of receivers. Amplitude and velocity changes on the ray paths can then be used to examine changes in material properties of the rock. Additional calculations using the velocities can determine the dynamic moduli, Young's modulus and Poisson's ratio, to give further indications of the properties of the rock through which the raypaths travel. Crack density and saturation are also determined for raypaths around the deposition hole. These values can be used to interpret the changes in velocities in terms of changes to the rock properties.

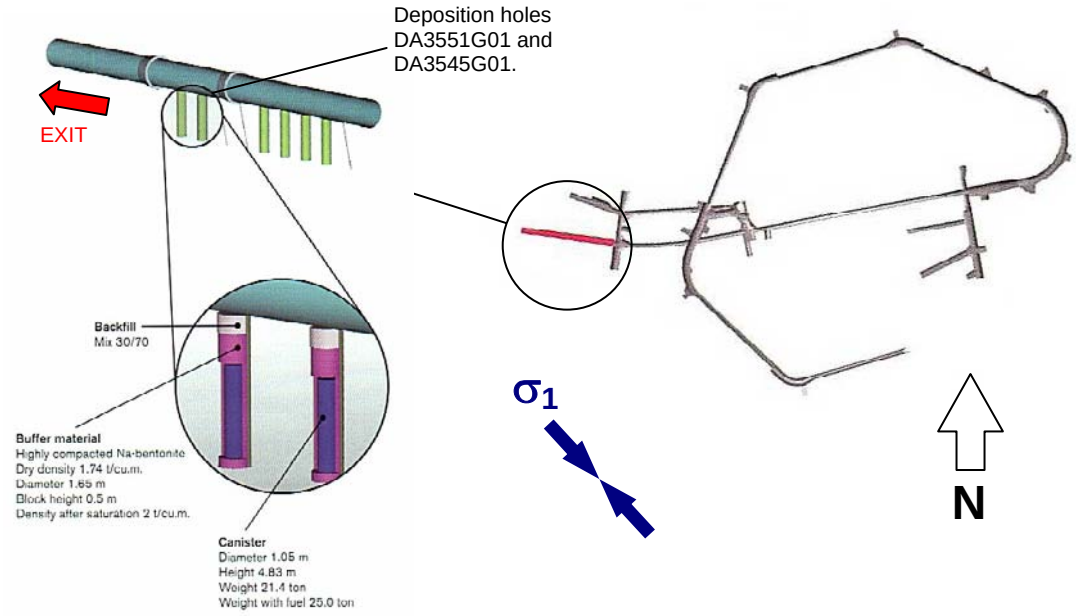

Figure 1-1: *Plan view of the experimental tunnels at the Äspö HRL and the location of the Prototype Repository. A schematic illustration of the final experimental set up is shown with canisters and bentonite clay buffer installed in the 1.75m diameter deposition holes. Note the entrance of the tunnel is towards the left. Graphics are modified from* SKB[1999].

This report presents the AE and ultrasonic methods used to investigate the rock response in the immediate vicinity of deposition hole DA3545G01 and presents an interpretation of the results obtained during monitoring up to March 2005. Deposition hole DA3545G01 was first excavated in September 1999. During the excavation period a temporary ultrasonic array was installed around the rock volume and removed after excavation [*Pettitt et al.*, 1999a]. A permanent ultrasonic array, with transducers

grouted into instrumentation boreholes, was then installed in the rock mass in June 2002. Ultrasonic monitoring has been conducted in two periods between 20th March and 9th October 2003, and 29th September 2004 to 31st March 2005. The gap in monitoring occurred when the ultrasonic acquisition system was used for another experiment in the HRL (Pillar Stability Experiment). Data to September 2003 has also been partially processed and reported by *Pettitt and Haycox* [2004] as part of the SAFETI project. In April 2003 heaters in the simulated waste canister were switched on causing temperatures to rapidly increase in the rock mass up to approximately 50°C at the rock wall. Figure 1-2 shows how temperature varies with distance from deposition hole wall, i.e. TR6045 is situated adjacent to the deposition hole wall and TR6041 is 2.2m into the rock. In November 2004 water drainage from the sealed Prototype tunnel was ceased causing a rapid increase in fluid pressures. The monitoring periods reported here thus capture the first 6 months of heating, when thermal gradients were at their highest, and record during a further 6 months when temperatures have reached a more steady state, but temporal changes in pressure were relatively large.

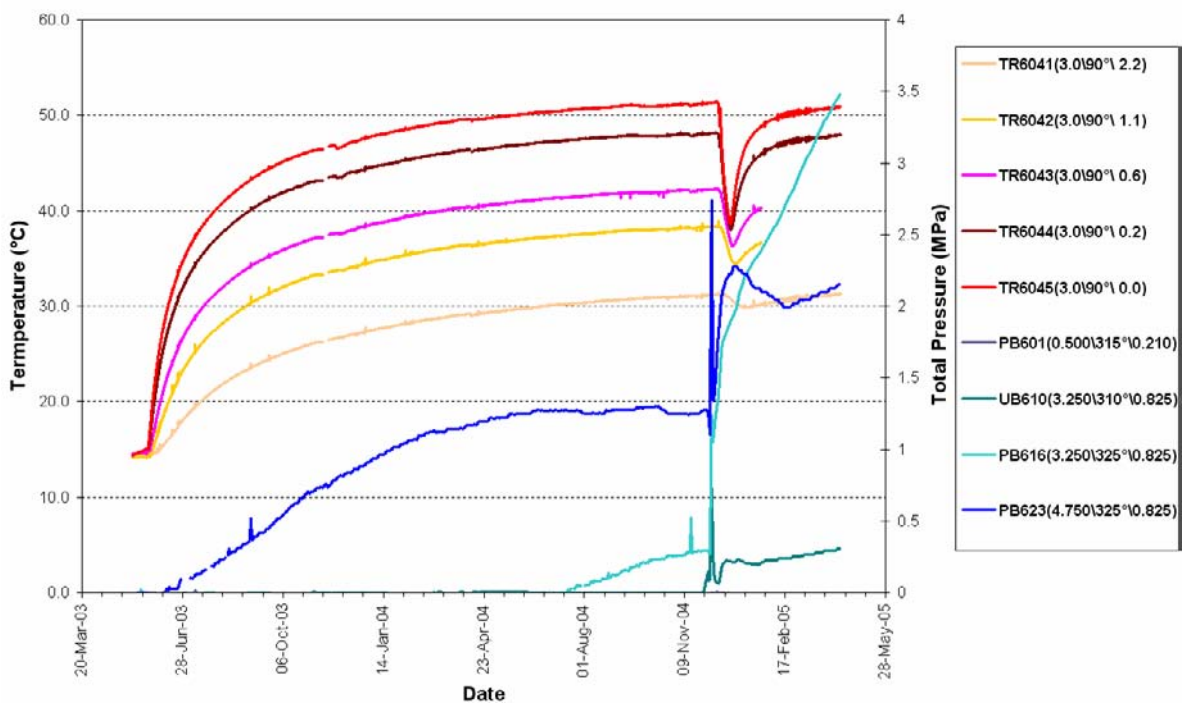

Figure 1-2: *Temperature (TR instruments) measured in the rock adjacent to the deposition hole and total pressure (PB and UB instruments) measured on the rock wall. Total pressure is the sum of pore pressure and bentonite swelling pressure.*

2 Specific Objectives

AE and Ultrasonic monitoring in the Prototype Repository Experiment has been performed with the following objectives:

- Produce accurate source locations for AEs so as to delineate the spatial and temporal extent of any brittle microcraking within the rock mass around the deposition hole and locate any movements on pre-existing macroscopic fractures.
- Conduct regular ultrasonic surveys to assess the effect of heating and other environmental changes on the velocity and amplitude of transmitted ultrasonic waves.
- Investigate changes in dynamic moduli and crack density to show how the properties of the rock volume around the deposition hole change through the experiment.
- Relate the AE and ultrasonic measurements to the measured *in situ* stress regime and other operating parameters such as temperature and fluid pressure.

3 Methodology

3.1 Data Acquisition

The ultrasonic array consists of twenty-four ultrasonic transducers configured as eight transmitters and sixteen receivers installed into four instrumentation boreholes. The transducers are fixed into the boreholes using specially designed frames (Figure 3-1) – two transmitters and four receivers per frame. The boreholes are vertical, 76mm in diameter and approximately 10 meters in length distributed around each deposition hole volume. The array has been designed so as to provide good coverage for AE locations and to provide 'skimming' ray paths that pass within a few centimetres of the deposition-hole void so as to sample the rock immediately adjacent to the deposition-hole wall. The layout of the instrumentation boreholes is shown in Figure-3-2 and described further in Table 3-1. Each of the ultrasonic transducers has a hemispherical brass cap fixed over its active face and is then spring-loaded against the borehole surface so as to obtain good coupling to the rock mass. The boreholes have then been filled with a slightly expansive grout so as to permanently fix the transducers in place, reduce the likelihood of damage to the transducers and to remove the borehole voids.

The piezoelectric transducers operate by converting a transient elastic wave into an electric signal or visa versa. The monitoring system is then operated in one of two modes. The first is used to passively monitor AE activity preferentially within the array volume. AEs release elastic energy in the same way as 'earthquakes' but over a very small scale. At these frequencies AEs have a moment magnitude (M_w) of approximately -6. They occur either during the creation process of new fractures within the medium, or on pre-existing fractures due to small scale movements. Each receiver has a frequency response of approximately 35-350kHz and contains a 40dB pre-amplifier. This minimises a reduction in signal-to-noise between the sensors and the acquisition system. The sensors have a vulcanised surround and a high pressure reinforced cable to protect them from water infiltration. In addition, polyamide tubes and *Swagelok* connectors have been fitted to the cables to reduce the likelihood of breakage.

Figure 3-1: *Top: Schematic diagram of the locations of all transducers on a single frame. Left: Photo of a section of the transducer assembly. Right: The transducer assembly during installation.*

Figure 3-3 shows a schematic diagram of the acquisition system used. Cables from each transducer pass through the pillar between the PRT and the G-tunnel. Data acquisition uses a Hyperion Ultrasonic System controlled by a PC, set up within a cabin provided by SKB. This has 16 receiving channels and 8 transmitting channels. An AE is recorded when the amplitude of the signal on a specified number of channels exceeds a trigger threshold within a time window of 5ms. The system then records the full-waveform signals from all 16 transducers. In this case a trigger threshold of 50mV on three channels was used. This allows the system to have sufficient sensitivity to record high quality data without recording an abundance of activity that cannot be processed due to very small signal to noise on only a few channels. The captured signals are digitised with a sampling interval of 1μs and a total length of 4096 data points. In general, low noise levels were observed (<2mV) giving high signal to noise and good quality data. AE monitoring is set to switch off during daytime working hours (6am-8pm) so as to minimise the amount of noise recorded from human activity.

A second operating mode actively acquires ultrasonic waveforms by scanning across the volume. This allows measurements of P- and S-wave velocities and signal amplitudes over a possible 128 different ray paths. By repeating these ultrasonic surveys at increments in time, a temporal analysis is obtained for the variation in medium properties. Ultrasonic surveys are conducted daily at 1am in order to measure changes in P- and S-wave signals. At that time of night, no human activity will cause noise that

can interfere with the signals received. A Panametrics signal generator is used to produce a high frequency electric spike. This is sent to each of the 8 transmitters in turn. The signal emitted from each transmitter is recorded over the 16 receivers in a similar fashion to that described above. An external trigger pulse from the signal generator is used to trigger the acquisition system and identifies the transmission start time to an accuracy of one sample point. In order to decrease random noise the signal from each transmitter is stacked 100 times.

Table 3-1: Boreholes used for AE monitoring of deposition hole DA3545G01.

SKB Borehole designation	ASC Borehole reference	Transducer Numbers
KA3543G01	1	T1, T2, R1-R4
KA3545G02	2	T3, T4, R5-R8
KA3548G03	3	T5, T6, R9-R12
KA3548G02	4	T7, T8, R13-R16

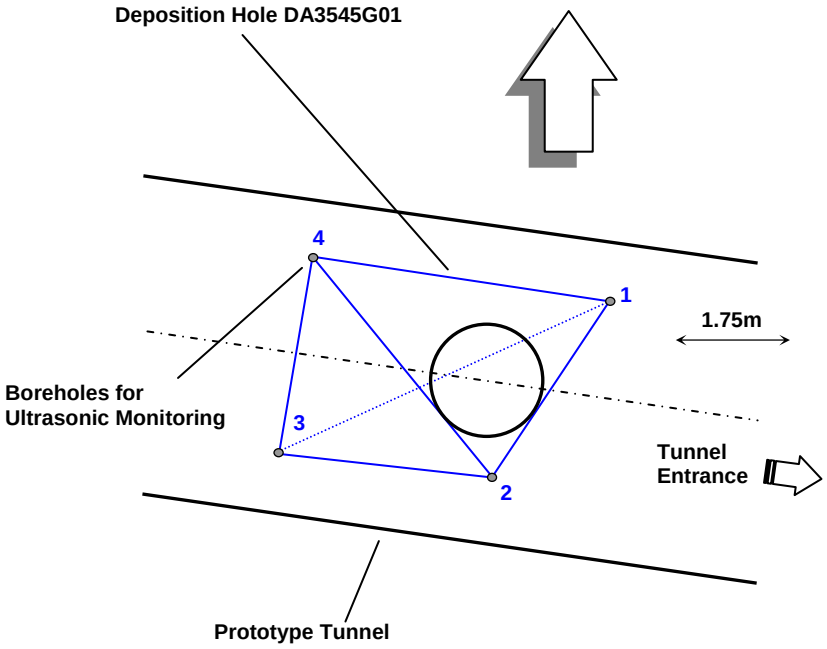

Figure 3-2: *Plan view of the array geometry for Deposition Hole DA3545G01 during heating in the Prototype Tunnel. The blue solid lines represent direct raypaths between sondes illustrating their 'skimming' nature. The blue dashed line represents a raypath that travels through the deposition hole.*

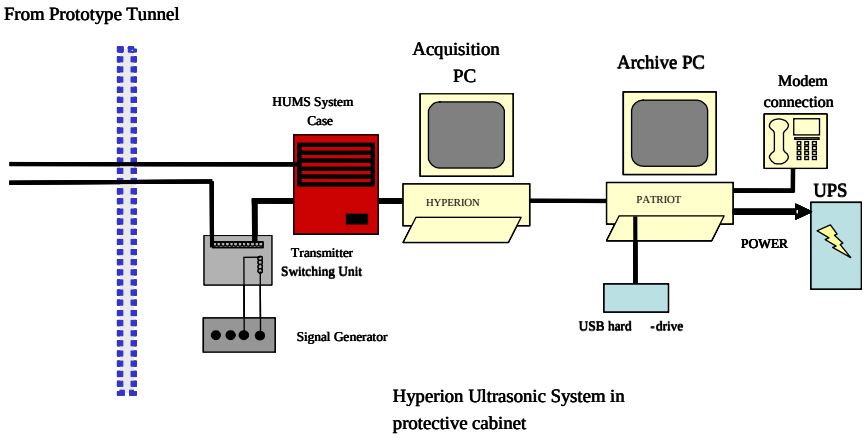

Figure 3-3: *Schematic diagram of the hardware used for the heating stage in the Prototype Repository. The ultrasonic pulse generator sends a signal to each transmitter and the resulting signal is recorded on each receiver. The receivers are also used to listen for AE activity. The archive PC is required to make a copy of the data for backup purposes.*

3.2 Processing Procedure

3.2.1 Overview

ASC's InSite Seismic Processor has been used to automatically process both the AE and ultrasonic survey data. Appendix 1A and Appendix 1B give the processing parameters used. *Pettitt et al.*[2005] provides a detailed description of this software.

3.2.2 Ultrasonic Data Procedure

The ultrasonic survey full-waveform data was initially stored with the AE data. This was first automatically sorted and the survey data extracted to a separate processing project. P and S-wave arrivals were manually picked for a 'reference' survey. Knowing the transmitter and receiver locations the ultrasonic velocity for each ray path was calculated with an estimated uncertainty of $\pm 30 m.s^{-1}$ (± 3 data points). A cross-correlation procedure was then used to automatically process subsequent surveys. This technique cross-correlates P- and S-wave arrivals from a transmitter-receiver pair with arrivals recorded on the same transmitter-receiver pair on the reference survey. This results in high-precision measurements of P- and S-wave velocity change with estimated uncertainties of $\pm 2 m.s^{-1}$ between surveys.

The main reason for the reduction of uncertainty is the dependency of manual picking on the user's judgement of the point of arrival. This can usually be quite indiscriminate because of random noise superimposed on the first few data points of the first break. Additionally, the procedure is run automatically without any loss of precision resulting in efficient waveform processing. The cross-correlation procedure then allows for a high-resolution analysis to be performed and hence small changes in velocity to be observed. This is extremely important when changes in rock properties occur over only a small section (5%) of the ray path.

Figure 3-4 gives example waveforms recorded from one of the transmitters during the heating phase of the experiment. Each waveform is first automatically picked to obtain an estimate of the P-wave or S-wave arrival. A window is then automatically defined around the arrival and a bell function is applied, centred on the automatic pick. The data at the ends of the window then have a much smaller effect on the cross-correlation. The windowed data is then cross-correlated [*Telford et al.*, 1990] with a similar window constructed around the arrival on the reference survey. The change in arrival time is then converted to a change in velocity knowing the manually-picked arrival time for the reference survey. Waveforms that do not provide automatic picks are not cross-correlated. This gives an automatic discrimination of signals that have very poor signal to noise ratios and could give spurious cross-correlation results from poor discrimination of the first arrival. During the automatic processing an arrival amplitude is also calculated from within a processing window defined by a minimum and maximum transmission velocity. This provides a robust measure of arrival amplitudes between surveys.

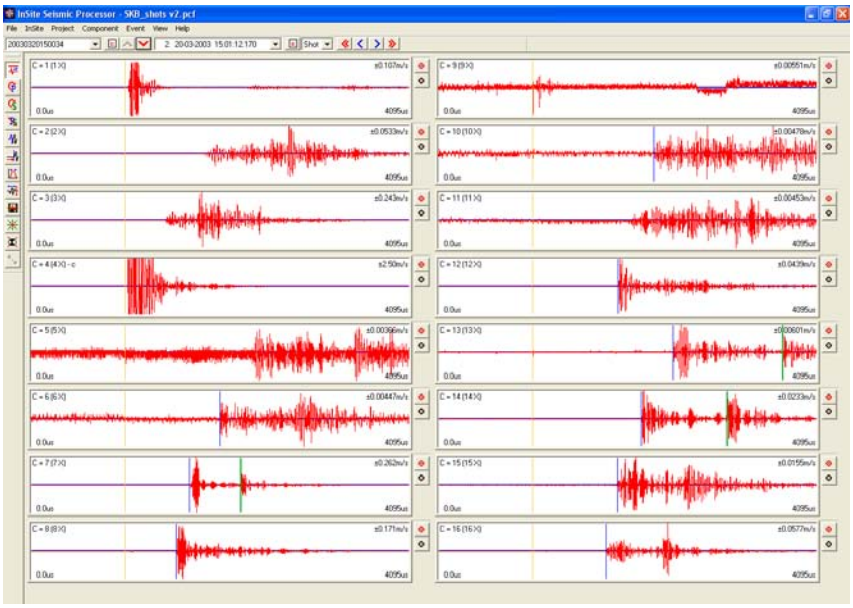

Figure 3-4: *Waveforms recorded from one transmitter on the array of sixteen receivers. The gold markers indicate the transmission time. The blue and green markers indicate picked P- and S-wave arrivals respectively.*

If V_P, V_S and the density, ρ have been determined, the dynamic Young's modulus *E*, and dynamic Poisson's Ratio, *v*, can be calculated using the Equation 1 and Equation 2.

$$E = \rho V_S^{\,2}\left(\frac{3V_P^{\,2} - 4V_S^{\,2}}{V_P^{\,2} - V_S^{\,2}}\right) \qquad \text{Equation 1}$$

$$v = \frac{V_P^{\,2} - 2V_S^{\,2}}{2\left(V_P^{\,2} - V_S^{\,2}\right)} \qquad \text{Equation 2}$$

V_P and V_S values are also used to model for crack density (c) and saturation (s) in the rock mass using the method of *Zimmerman and King*[1985]. The crack density parameter is defined by the number of cracks (penny-shaped) per unit volume multiplied by the mean value of the cube of the crack radius (Equation 3). This method assumes the elastic modulus E and v in the damaged material normalized to the undisturbed material, decrease exponentially with crack density. Also assumed are the shear modulus (μ) is unaffected by s, and the bulk modulus (k) increases linearly with s, equalling that of uncracked rock when s=1. Equation 4 shows the calculation used to determine saturation.

$$c = \frac{9}{16}\ln\left(\frac{2\mu}{E_0 - 2\mu\nu_0}\right) \qquad \text{Equation 3}$$

$$s = \frac{k(c,s) - k(c,0)}{k_0 - k(c,0)} \qquad \text{Equation 4}$$

The calculations require an estimation of the completely undisturbed rock (i.e. an unsaturated, uncracked, intact rock mass). This study assumes values of V_{0P} = 6660 m/s, and V_{0S} = 3840 m/s for the undisturbed material taken from laboratory tests on a similar granite, summarized in *Maxwell et al.*[1998]. A value of 2650 kg m^{-3} is presented by *Pettitt et al.*[2002] for the density of the rock mass.

The calculations of Young's Modulus and Poisson's ratio from measured velocities makes an assumption of an isotropic elastic medium. Under this assumption a rock can be completely characterised by two independent constants. One case of an isotropic elastic medium is a rock with a random distribution of cracks embedded in an isotropic mineral matrix. Under the application of a hydrostatic compressive stress, the rock will stay isotropic but become stiffer (which will become characterised by increased velocity V_P, V_S and therefore increased Young's modulus). In contrast, under the application of a uniaxial compressive stress, cracks with normal's parallel or nearly parallel to the applied stress will preferentially close and the rock will take on a transversely isotropic symmetry. Under this situation P- and S-wave velocities become variable with orientation. The crack density and saturation calculations also assume an isotropic elastic medium.

It should be noted that E and v calculated in this report are dynamic measurements due to the small strains exerted on the rockmass at high frequencies from the passing ultrasonic waves. Static E and v measurements, made from uniaxial laboratory tests on rock samples, may be different from dynamic values – even if sample disturbance is minimal – due to the larger strains exerted over relatively long periods of time.

3.2.3 Acoustic Emission Procedure

The procedure used to process the AEs in this reporting period has been undertaken as follows:

1 Calibration surveys from the installation phase (when the deposition hole was open) have been used to optimise an automatic picking and source location algorithm and check location uncertainties. For the heating phase, ASC's InSite seismic processing software was used.

2 Where possible, P- and S-wave arrival times are measured for each AE using the automatic picking procedure.

3 AEs with ≥6 P-wave arrival times are input into a downhill-simplex location algorithm [*Pettitt et al.*, 2005]. This has the option of incorporating either a three-dimensional anisotropic velocity structure or an isotropic structure. Velocities calculated from the ultrasonic surveys are used.

4 The waveforms from all events were visually inspected to ensure they were 'real' acoustic emissions. Events were removed if they had the appearance of noise spikes (increase in amplitude is recorded on all channels at the same time) or they were the result of human noise (long period events that occur at close intervals during the day).

5 The acoustic emissions that remain had their arrivals manually checked. Any events that locate outside the expected region of activity were further checked to ensure accuracy. Experience from previous studies around deposition holes showed that large source location errors were produced if significant portions of a ray path passed through the excavated deposition hole void. This only becomes a problem for the largest AEs. AEs were reprocessed with these ray paths removed.

6 Finally, a filter is applied to remove all AEs with a location error greater than 1.0.

During the equipment installation phase, calibration shots have been undertaken to assess the sensitivity of the system to 'real' AEs and to determine the accuracy with which real events could be subsequently located by the array of sensors. A series of test 'shots' were performed on the wall of deposition hole DA3545G01 (Figure 3-5). The shots consisted of undertaking 10 'pencil lead breaks' and 10 hits with a screw-driver at 1 metre intervals down 4 lines along the deposition hole wall. The pencil-lead tests involved breaking the 0.5 mm lead from a mechanical pencil against the borehole wall. This is a 'standard' analogue for an AE as it generates a similar amount of high-frequency energy. An example of a pencil lead break test is shown in Figure 3-6. This was made at 6 metres below the tunnel surface on the deposition hole wall at a point adjacent to borehole KA3548G02. This corresponds to an AE source dimension on the millimetre scale (grain size).

The screw-driver hits provided a good amplitude signal for assessing the accuracy with which events can be located within the volume surrounded by the array. the results from one processed set of locations for a line of shots down the deposition hole wall. This shows that the array is able to locate events with good accuracy and consistency within an estimated uncertainty of approximately 10cm.

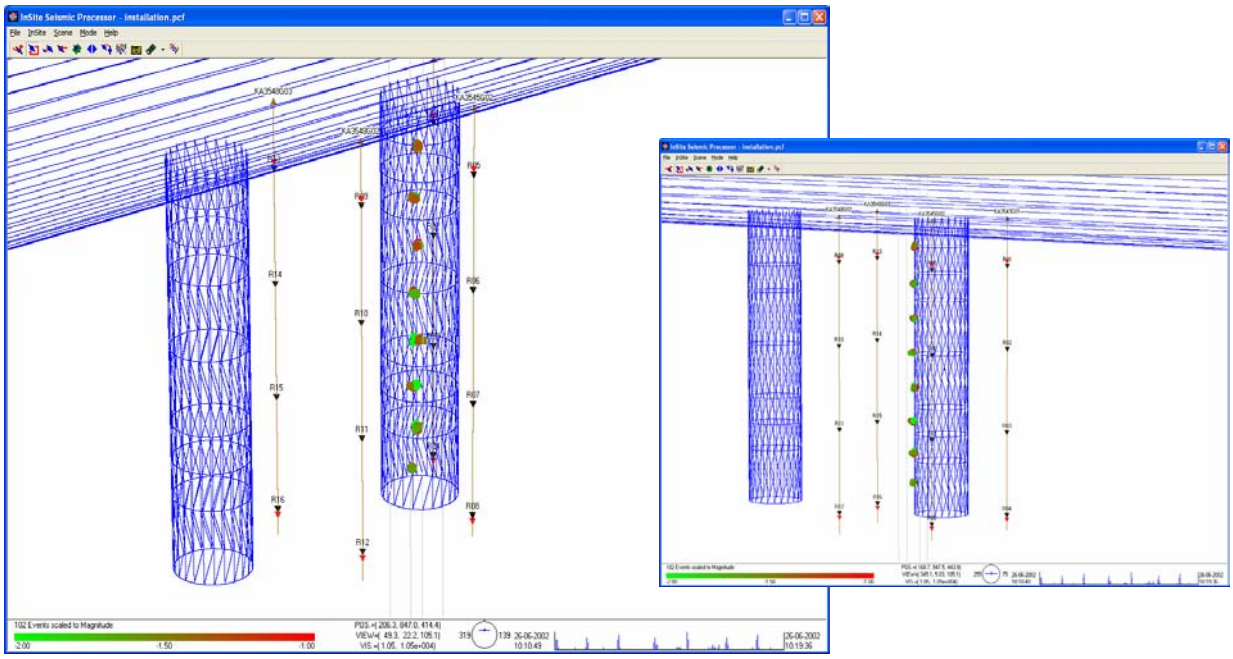

Figure 3-5: *Locations of calibration shots obtained from a series of tests at 1 metre intervals down the wall of deposition hole DA3545G01. The two views show that these line up and are located close to the surface of the hole.*

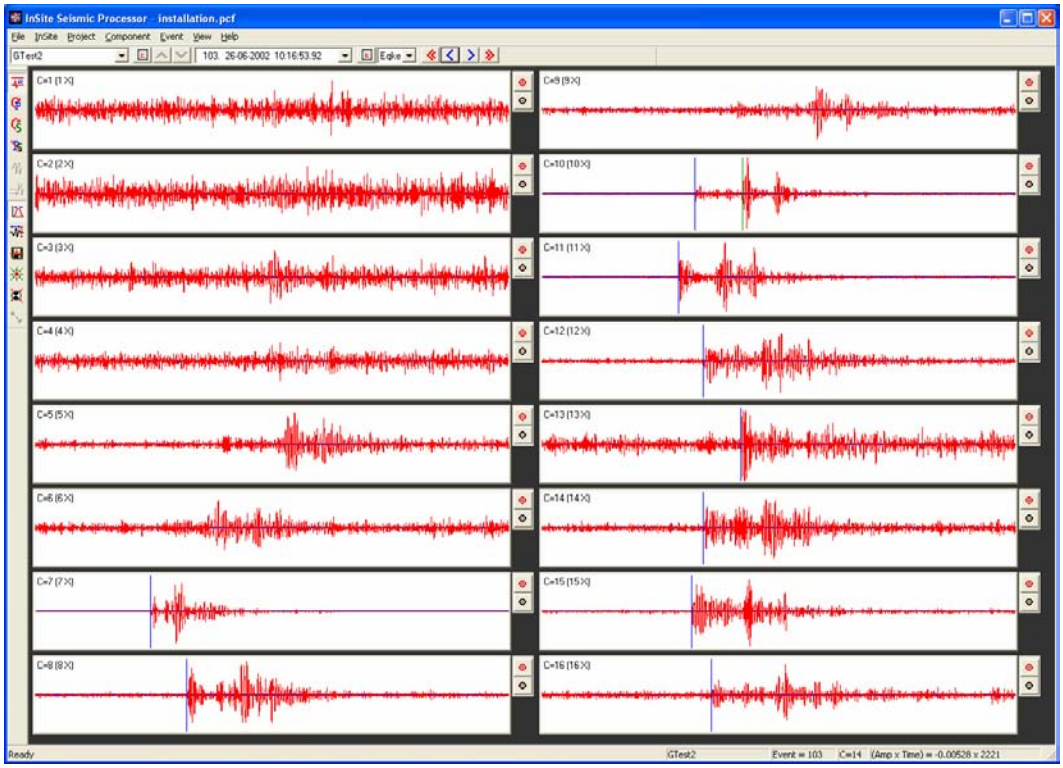

Figure 3-6: *Example waveforms from each of the 16 receiving channels for a 'pencil-lead break' test undertaken against the Deposition Hole (DA3545G01) wall 6 metres below the tunnel floor.*

4 Stress Field and Ultrasonic Measurements at the HRL

4.1 Stress Field

The rock mass at the 450m level is predominantly massive Äspö diorite. *Patel et al.*[1997] have performed detailed mapping of discontinuities in the Prototype Repository tunnel. Two main discontinuous sets of sparse, en-echelon, fractures were observed. The principal fracture set is steeply dipping orientated to the West-Northwest (Figure 4-1a). This is regarded as the main water-bearing set. Sparsely located fractures are also observed with sub-horizontal dips and with steeply dipping North-south orientations. Similar fracture sets were found in the ZEDEX tunnels at the 420m level and are believed to be characteristic of the HRL volume.

Leijon[1995] summarises the stress magnitudes and orientations measured in boreholes at various locations down the HRL ramp using a CSIRO cell. Orientations are summarised in Table 4-1Note there is a strong agreement between the maximum principal stress (σ_1) and the orientation of the principal fracture set. σ_1 is at 33^o azimuth from the tunnel orientation (Figure 4-1b), which has an axis orientated 98^o azimuth from North and 1.2^o plunge towards the east. Note there is a strong agreement between the maximum principal stress (σ_1) and the orientation of the principal fracture set. *Young et al.*[1996] note this agreement at the HRL and elsewhere

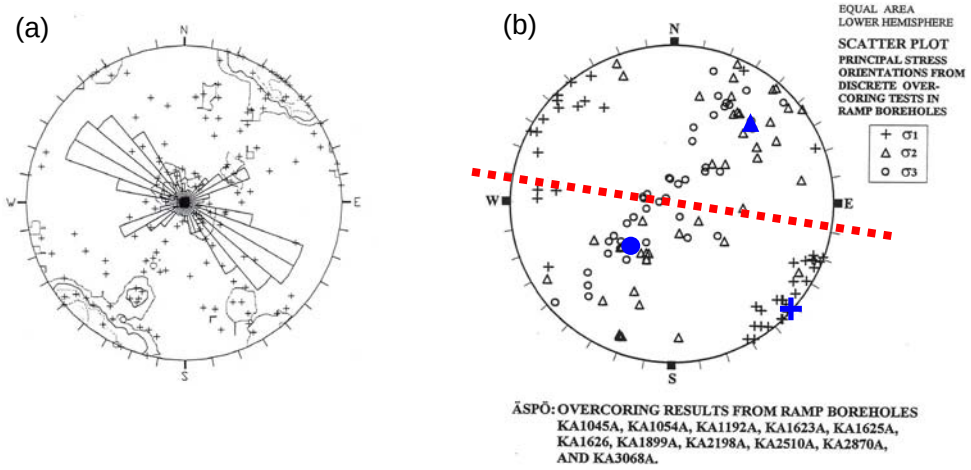

Figure 4-1: *a) Pole, contour and rosette plot of joints from detailed mapping of the PRT performed by* Patel et al.*[1997]. b) Principal stress orientations measured from boreholes excavated from the HRL ramp (black markers) and summarised in* Leijon*[1995]. Blue markers are far-field stress measurements (Table 4-1). The dashed line is the azimuth of the PRT.*

In previous studies at the HRL, AEs have been a good indicator of the local stress conditions. In the ZEDEX experiment AE distributions were related to excavation stresses induced by the tunnel excavation method employed [*Young et al.*, 1996].

During excavation of deposition holes in the Canister Retrievel Test and the Prototype Repository, AE locations were shown to be preferentially orientated to the *in situ* stress field [*Pettitt et al*., 1999b; *Pettitt et al*., 2003a; *Pettitt et al*., 2003b]. This is further described in Section 4.2.1. *Pettitt et al.*[2000] further discusses the stress field and presents elastic modelling of stresses around the deposition holes during excavation of the Prototype Repository holes (see Section 4.2.1).

More recently, *Staub et al.*[2004] have presented detailed geological mapping of the TASQ tunnel in which the Pillar Stability Experiment has been undertaken. The fracture sets identified are found to coincide well with the geological data set of the Äspö Hard Rock Laboratory. Extensive stress measurements have been undertaken around the site of the experiment [*Staub et al.*, 2004]. When complemented with convergence measurements obtained during excavation of the deposition holes, back calculations were performed to find the best fit stress field (Table 4-2). The second principle stress is vertical and approximately 25% higher than the weight of the overburden. The maximum principal stress agrees well with the dominant orientations of the mapped geological structures observed and relates favourably with results from the Prototype Repository.

Table 4-1: Measured stress field: Principal stress values for the 420m level. These results are an average stress tensor for the 420m level calculated from data originally reported by *Leijon*[1995].

Stress Component	Magnitude(MPa)	Trend (^{o})	Plunge (^{o})
σ_1	32	131	0
σ_2	17	41	25
σ_3	10	229	65

Table 4-2: Measured Stress Field: Principal stress values for the TASQ tunnel from Staub et al.[2004].

Stress Component	Magnitude(MPa)	Trend (^{o})	Plunge (^{o})
σ_1	30	310	0
σ_2	15	90	90
σ_3	10	208	0

4.2 Previous Deposition-hole Monitoring at the HRL

4.2.1 Deposition Hole Excavation in the Prototype Repository

Pettitt et al.[1999a] presents results from acoustic emission and ultrasonic monitoring of the excavation of two canister deposition holes in the Prototype Repository. Deposition hole excavation occurred in the period April to September 1999, during which time temporary ultrasonic arrays were installed around DA3551G01 and DA3545G01. AE monitoring was used with the aim of delineating zones of stress-related fracturing around the deposition hole perimeter, and to observe the effect of excavation on pre-

existing macroscopic fractures. Changes in ultrasonic velocities, measured every hour, were used to investigate stress disturbance of the rock mass over a broader time and volume than the AE scale, and to quantitatively measure the accumulation of fracturing in the damaged zone. Monitoring was also performed during excavation of two deposition holes in the Canister Retrieval Test at the 420m level and showed consistent results to the Prototype Repository [*Pettitt et al.*, 1999b].

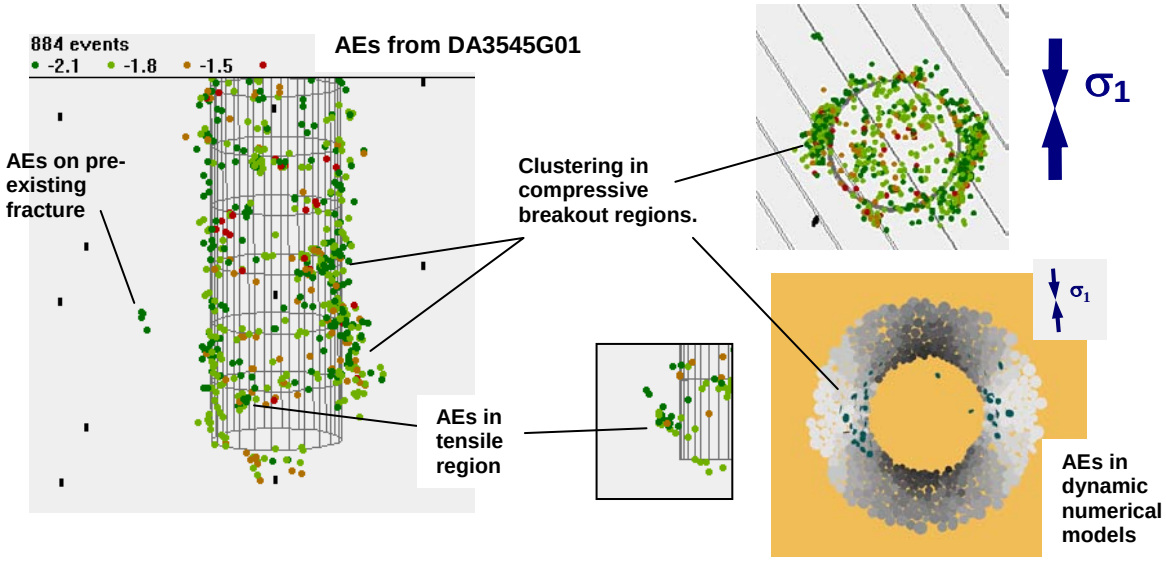

Figure 4-2: *AE locations around DA3545G01 at the Prototype repository during excavation of the deposition hole. Plan view shows the orientation of the principle stress with respect to the location of AEs. The induced fracturing is demonstrated in the numerical model simulating the excavation.*

A total of 2467 AE triggers were obtained during monitoring of the two deposition holes. Of these 1153 were located. There was significantly more AE activity around the second deposition hole (labelled DA3545G01) than the first (DA3551G01). This difference is likely to depend upon intersection of the excavation with a greater number of pre-existing fractures. These fractures may be preferentially located in the side wall of the deposition hole or preferentially orientated to the *in situ* stress field. Breakout fracturing has been observed with AEs distributed mainly in regions orthogonal to the maximum principal stress, σ_1. This is consistent with observations from the Canister Retrieval Tunnel and from dynamic numerical models. AEs, and hence microcrack damage, are shown to locate in clusters down the deposition hole and not as a continuous 'thin skin' (Figure 4-2). *Pettitt et al.*[2000] showed that these clusters are associated with weaknesses in the rock mass generated by excavation through pre-existing fractures. AE results from both the Prototype Repository and the Canister Retrieval Tunnel show that damage in the side wall of the deposition holes depends significantly on these pre-existing features. The *in situ* stress field is a contributing factor in that induced stresses are sufficiently high to create damage in these weakened regions although not sufficiently high to create significant damage in the rock mass as a whole.

Baker et al.[1999] showed results from PFC^{3D} (Particle Flow Code) modelling of the excavation phase of the experiment. An example of modelling displacements and cracking during excavation of a single round is shown in Figure 4-2. 92 cracks formed during the 4m vertical excavation modelled. Most were oriented approximately parallel to the maximum stress direction (North-South in this case). This agreed with the actual recorded AEs which are also presented in Fifure 4-2 for comparison.

The damaged zone in the breakout regions was mapped by AEs extending 20-30cm into the side wall. The scale of fracturing, from calibration studies, is believed to be of the order of millimetres in dimension. Changes in ultrasonic velocities are shown to be approximately 10-30m.s^{-1} through regions of unloaded compressive stress - or tensile stress. These changes occur during excavation of a few rounds as the deposition hole passes the ray path, as demonstrated in Figure 4-3. This agrees with the time dependency of AEs showing that stress-induced fracturing is most severe in the first 24 hours after excavation of a round. The mean change in velocity for 'skimming' ray paths, that pass the excavation by only a few centimetres, is approximately -15m.s^{-1}. This is an identical result to that obtained in the Retrieval Tunnel and describes a 15% reduction in dynamic Young's modulus in the observed excavation damaged zone. Changes in velocity are observed to be dependent on the ray path orientation relative to the deposition hole. Ray paths that pass through regions of low compressive stress describe larger changes in velocity than ray paths through regions of high compressive stress (Figure 4-4). This is due to fractures in the unloaded regions being preferentially opened.

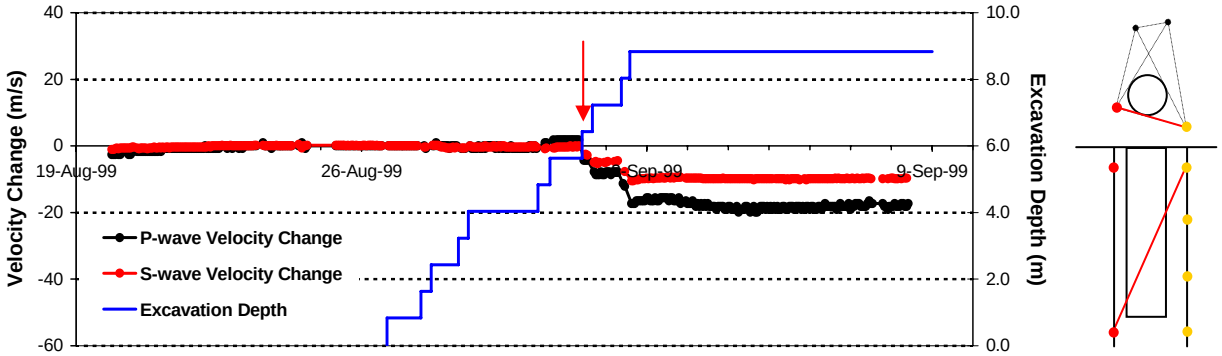

Figure 4-3: *Change in P- and S-wave velocity during deposition hole excavation along a selected raypath. The red arrow indicates the time excavation depth passes the direct raypath between transmitter and receiver.*

Pettitt et al.[2000] produced three-dimensional stress models for the Prototype Repository (Figure 4-5) and showed the AE distributions to be consistent with an average *in situ* stress tensor calculated from *Leijon*[1995] (σ_1 has an azimuth of 131^{o}EofN). This relationship holds for all the deposition holes monitored in both the PRT and the Retrieval Tunnels. AEs located in the floor of the deposition hole can also be explained by the localisation of high stress concentrations from the measured stress field. *Pettitt et al.*[2000] also tested whether two deposition holes result in a combined disturbance. These models show that the induced stress fields of the two neighbours are linked. When three deposition holes are excavated in a line the central deposition hole has a loading of +2.5MPa (approximately 3%), in regions parallel to the tunnel axis,

compared to if it had no neighbours. This combined disturbance is related to the distances between the two deposition holes, the rock mass behaviour, the geometry of the tunnel above, and the orientations of the excavations with respect to the stress field, and so is likely to be different for different excavation designs.

Source mechanism solutions for 56 AEs obtained during excavation of the deposition hole have been calculated by *Pettitt et al.*, [2000]. All of these AEs are located within the first few centimetres beneath the floor of the deposition hole. These mechanisms have a dominant component of frictional sliding (double-couple), although there are also often significant (>30%) components of isotropic and CLVD decompositions that suggest more complex failure than just simple shear (Figure 4-6). The source mechanisms show that the AEs are occurring on micro-fractures that are preferentially orientated sub-horizontal, or sub-parallel to the excavation face. The source mechanisms obtained have slip vectors orientated parallel to the maximum principal stress although there is an ambiguity in their sense of slip; that is the slip vectors (slip of the upper surface of the micro-fracture relative to the lower surface) are orientated either northwest or southeast. The microcracks generating the AEs are likely to be rough surfaces at the scale of the AE source dimension (millimetres), with the microcracks travelling around and between grains. This easily explains any small variations in fracture orientation.

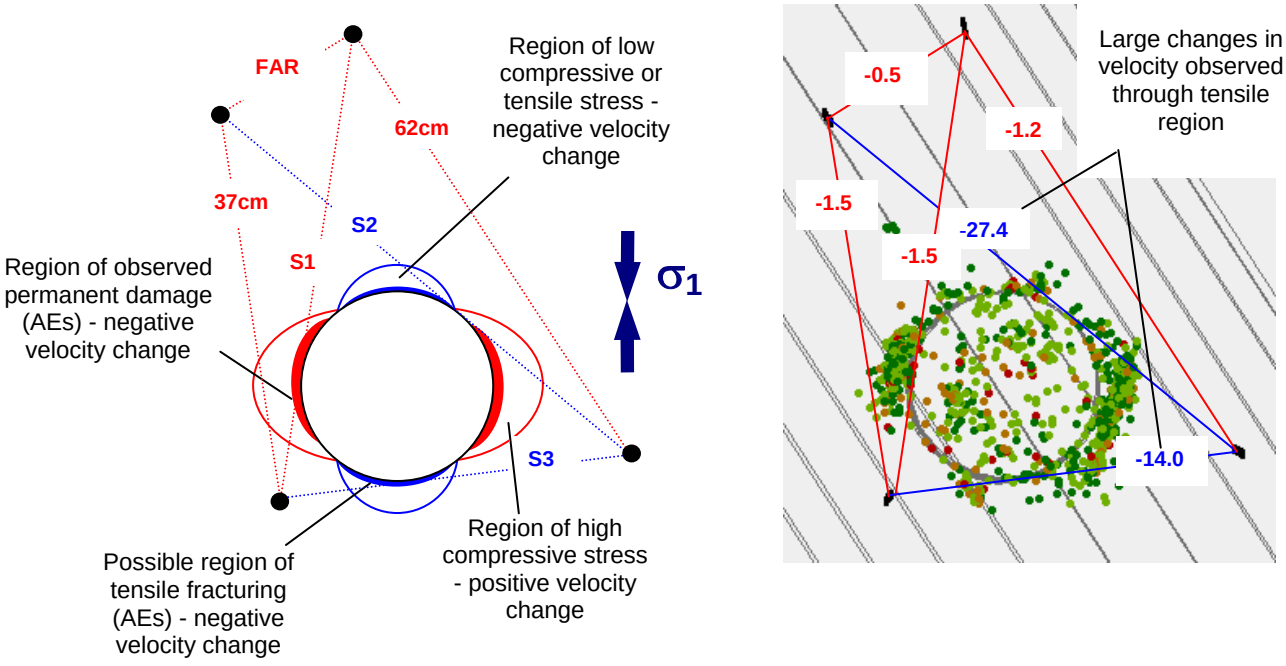

Figure 4-4: *Plan view of deposition hole DA3545G01 with located AEs and superimposed mean velocity changes during excavation (left); and interpretation of results in terms of disturbed and damaged regions (left).*

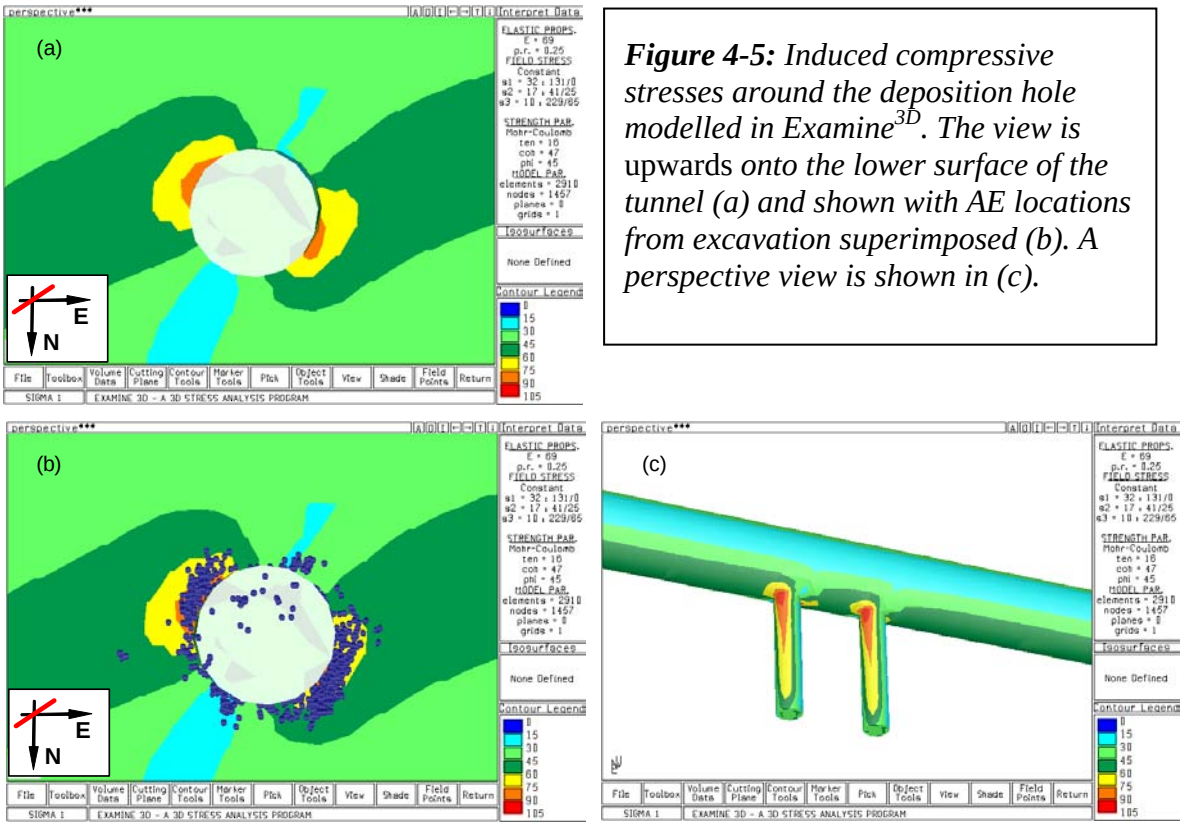

Figure 4-5: *Induced compressive stresses around the deposition hole modelled in Examine*^{3D}*. The view is* upwards *onto the lower surface of the tunnel (a) and shown with AE locations from excavation superimposed (b). A perspective view is shown in (c).*

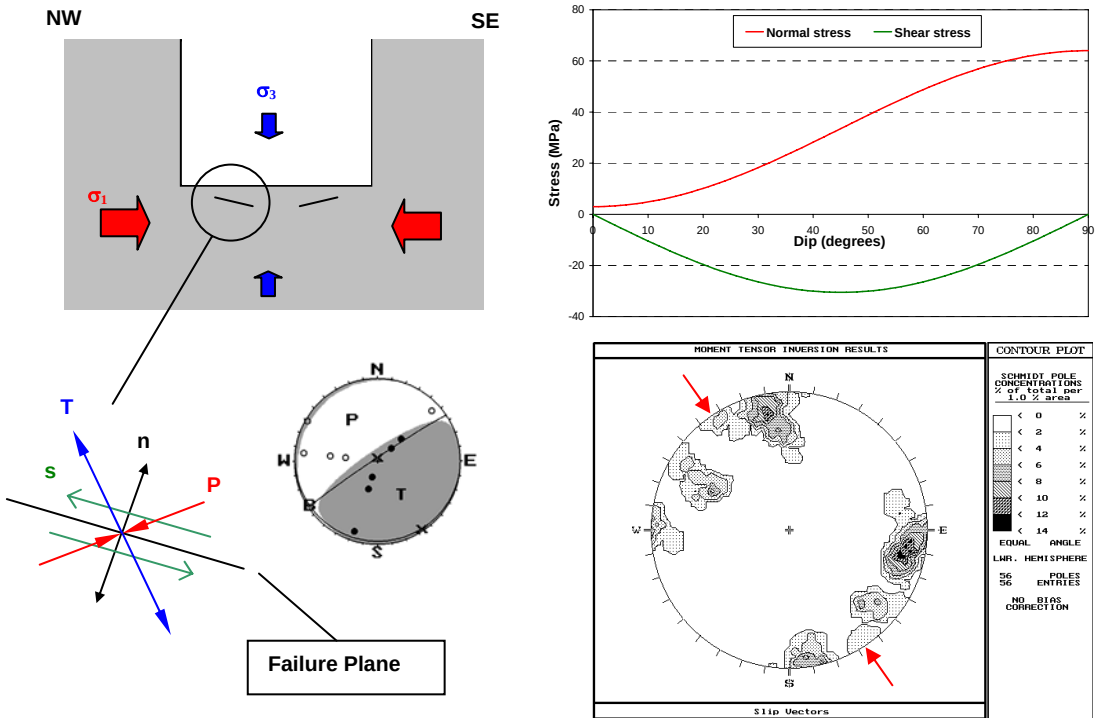

Figure 4-6: *AE source mechanism results show a dominant mechanism type (left) on sub-horizontal fractures. Slip is activated due to low normal stresses (upper right). Slip vectors are preferentially orientated in the southeast-northwest quadrants of the lower hemisphere validating measured plane dip that enables slip to occur and in turn causes this bi-directional effect.*

4.2.2 Monitoring of the Pillar Stability Experiment

The Äspö Pillar Stability Experiment (APSE) was undertaken to demonstrate the current capability to predict spalling in a fractured rock mass using numerical modelling techniques, and to demonstrate the effect of backfill and confining pressure on the propagation of micro-cracks in rock adjacent to deposition holes within a repository [*Andersson*, 2002]. An ultrasonic acquisition system installed by Applied Seismology Consultants Ltd. (ASC) provided acoustic emission and ultrasonic survey monitoring throughout the various phases of the experiment. *Haycox et al.*[2004] reported the results of monitoring -- a summary of which is presented below.

A pillar was produced by excavating two 1.8m diameter deposition holes 1m apart. These were bored in 0.8m steps using a Tunnel Boring Machine (TBM) specially adapted for vertical drilling. The first deposition hole, DQ0066G01, was drilled in December 2003. Preceding this a period of background monitoring was performed so as to obtain a datum for the results. The hole was then confined to 0.8MPa internal pressure using a specially designed water-filled bladder. The second deposition hole, DQ0063G01, was excavated in March 2004. Heating of the pillar was performed over a two month period between ending in July 2004, when the confined deposition hole was slowly depressurised. Immediately after depressurisation the pillar was allowed to cool with cessation of monitoring occurring a month later.

Ultrasonic velocities measured prior to the excavation of the deposition holes gave a mean P-wave velocity of 6051m.s^{-1}, and mean S-wave velocity of 3394m.s^{-1}, in a weakly (1.5%) transversely isotropic rock mass. This has a fast direction orthogonal to the tunnel direction (north west to south east and around to the vertical). The slow velocity direction is thus parallel to the tunnel, orthogonal to the major fracture set and maximum principal stress direction. Ultrasonic velocity surveys were undertaken regularly during the whole of the APSE. Velocity and amplitude results, for every raypath that could be processed, are provided with this document. These include 54 separate P-wave velocity measurements and 23 S-wave velocity measurements on 350 surveys conducted over the monitoring period.

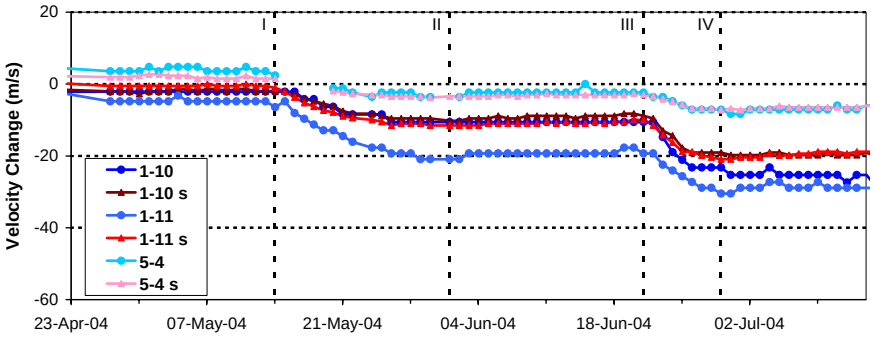

Figure 4-7: *Velocity change graph for a selection of raypaths passing through the centre of the pillar. Markers I to IV represent times when the heater power settings were changed. I and III are times when power was increased.*

Skimming ray paths, that passed through excavation damage close to the deposition holes (as imaged by the AE results), often showed a significant decrease in velocity during excavation of between 5 to 30m.s^{-1}. Some ray paths also exhibited an increase in velocity of approximately 10m.s^{-1} over the days following excavation. An increase could be the result of increasing stresses in some volumes of the rock mass acting to close microfractures (the ray paths also pass through the induced zones of high compressive-stress). The velocity increases may counteract any decreases in velocity caused by new fracturing and result in a net increase. During the heating phase there is often a clear decrease in velocity in two stages that correlates very well with the AE activity and known changes in the thermal output of the heaters. Ray paths that travel through the centre of the pillar show a similar response, although of lower magnitude (Figure 4-7). The velocity decreases could be related to a desaturation of the rock mass, new fracture growth or expansive stresses causing an opening of pre-existing fractures. The latter is unlikely as modelled increasing compressive stresses will act to close preferentially-orientated fractures.

A total of 36,676 AE triggers were recorded over the reporting period between 13th October 2003 and 14th July 2004. Figure 4-8 displays the 15,198 of these that have produced AE locations. The AE data set shows an intense clustering of events located along the length of the deposition holes to approximately 1m from their floors. Clustering of events is primarily contained in a damage zone orthogonal to the maximum principal stress, represented by a semi-circle of tightly packed AEs extending from the edge of each hole approximately 20cm into the pillar. Very few events are situated in the centre of the pillar, although clusters of events occur in the top metre of the pillar volume in two sub horizontal features that cross the pillar. The uppermost feature is believed to be associated with the rock floor of the tunnel, beneath the concrete roadbed, and the lowermost feature is associated with a mapped shear zone.

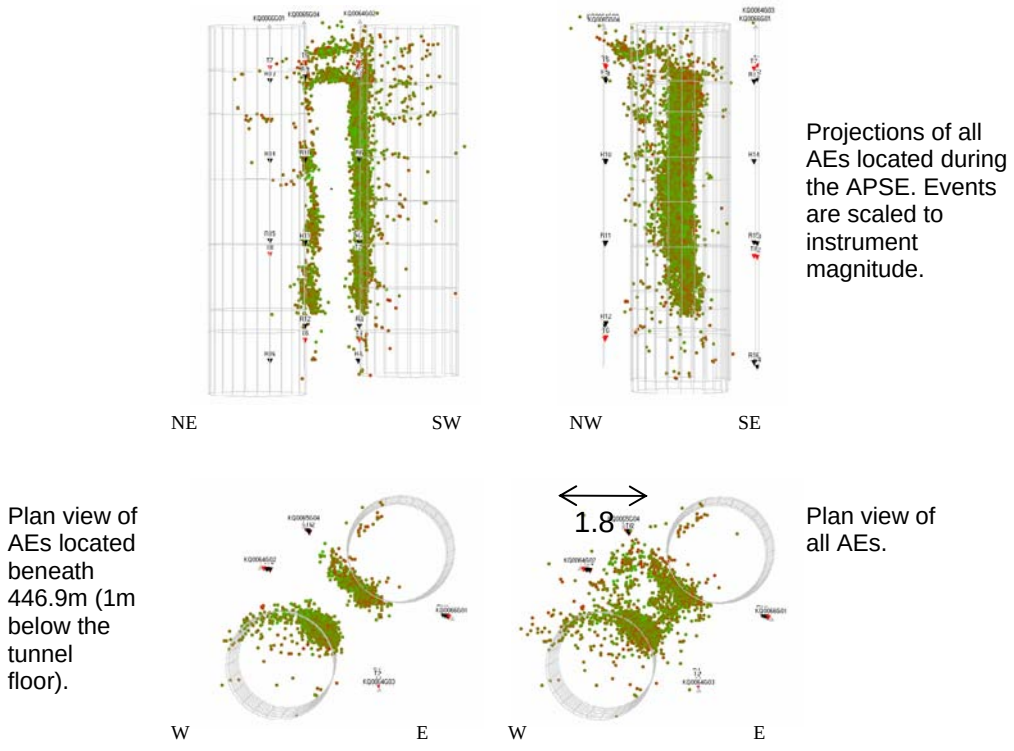

Figure 4-8: *Various projections of AE locations at the APSE. See comments for descriptions of individual diagrams.*

Acquisition system triggers, channel hit counts and processed locations all show a consistent temporal distribution for the AE activity. During background monitoring, preceding excavation of the first deposition hole, no activity was recorded. Excavation of the two deposition holes produces increased activity. This is much larger for the second deposition hole when the pillar is formed. The activity decays away after excavation over approximately two weeks. Heating of the pillar causes increased activity occurring in two sets between May and July 2004. The sets of activity correspond to two heating periods; the second period being caused by an increase in thermal output by the heaters used.

The clustering of AE locations is observed to migrate along the pillar walls of the two deposition holes during the various phases of the experiment. During excavation of DQ0066G01, the largest amount of activity occurs in a cluster at 3.6m depth, which qualitatively correlates with spalling observed in the deposition hole. The cluster occurs 1.2m behind the advancing deposition-hole face and is probably a result of increasing stresses in a weaker part of the rock mass during deeper excavation. During excavation of DQ0063G01, a zone of intense AE activity occurs, extending from close to the top of the deposition hole. and migrating down the hole to a depth of approximately 2.5m. The highest event rates are observed after excavation is completed. The AE activity correlates well with a zone of breakout damage observed in the open hole after excavation. Similar amounts of high activity are not observed in the confined deposition hole during this phase, suggesting the confinement pressure applied here is sufficient to inhibit breakout occurring.

During heating of the pillar a consistent lag of a few days (3-4) is observed between the heaters being adjusted and when the rock responds to the adjustment. The events initially cluster in previously active regions down the open deposition hole, DQ0063G01. As the temperature increases this cluster grows larger, extending upward to the rock floor of the tunnel and then migrating downward reaching a depth of approximately 5m below the tunnel floor.

5 Results

5.1 Ultrasonic surveys

5.1.1 Overview of Parameters

Figure 5-1 shows the three-dimensional velocity structure for the survey recorded on 20th March 2003 at the start of the first monitoring period. A total of 64 ray paths could be processed for P-wave velocities and 23 for S-wave velocities. The structure is principally isotropic but with some localised heterogeneities. These could be a combination of measurement uncertainty (estimated at ±30m.s^{-1} for absolute velocity measurements) and localised effects from the deposition hole (excavation damage zone and stress field). The average P-wave velocity is 5909m.s^{-1} and the average S-wave velocity is 3315m.s^{-1}. This is consistent with the average velocities measured after excavation by *Pettitt et al.*[1999a].

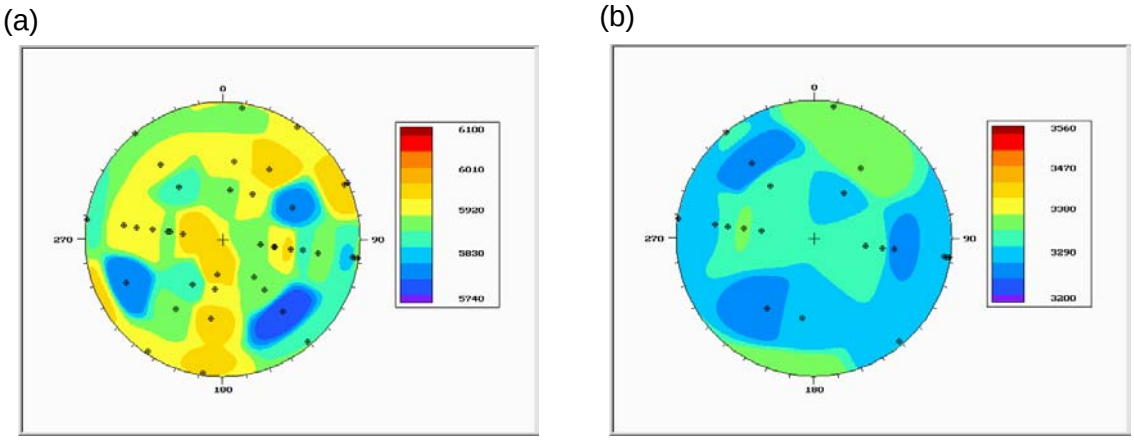

Figure 5-1: *Lower-hemisphere stereonets of a) P-wave velocity and b) S-wave velocity for the reference survey on 20th March 2003. The ray path orientations are shown by black markers.*

Figure 5-2 shows the three-dimensional velocity structure for the survey recorded on 8th December 2004. The velocity scales for P- and S-wave velocity are the same as in Figure 5-1. A large increase has occurred along the majority of the raypaths, across a range of orientations and declinations. The average P-wave velocity is 5974 m.s^{-1} and the average S-wave velocity is 3343m.s^{-1}. These changes will be discussed further below and can be explained by temperature increases in the rock from heating of canisters in the deposition holes, and pressure increases as a result of closing drainage from the Prototype Repository.

Measurements from temperature and pressure instruments located in, and around the deposition hole, provide an indication of the major environmental changes occurring during this reporting period. Figure 5-3 shows temperature changes in the rock around the deposition hole. On the 25th May 2003 temperature starts to increase after heaters are switched on. The first stage of heating is rapid, and temperatures increase quickly, especially for the sensors located closest to the deposition hole. At the end of the first monitoring period (October 2003) the temperature at the deposition hole wall is

approximately 45°C. From November 2003, temperature increases at an almost constant rate on all instruments until December 2004. At this point there is a short-term reduction in temperature when heaters were switched off due to electrical problems with the heaters [*Johannesson*, 2005]. By the end of the second monitoring period the maximum temperature measured on the deposition hole wall was 52.8°C. A detailed look at how variation in temperature effects velocity and amplitude is presented in Section 5.1.2.

On 1st November 2004, drainage from the tunnel was closed resulting in an increased pressure in the tunnel. Changes to total pressure, the sum of the bentonite swelling pressure and the pore water pressure, have been measured at various locations in the Prototype Repository. An increase in total pressure is recorded in the tunnel backfill above the deposition hole immediately after drainage is closed (Figure 5-4a). As time progresses the rate of pressure change increases reaching a maximum on 1st December 2004. Pressure in the rock, adjacent to the deposition hole displays little change prior to 4th December 2004 (Figure 5-4b). On this date there is a rapid increase in total pressure experienced on three of the four instruments. On 6th December 2004 the canister in hole DA3545G01 is observed to have been damaged [*Johannesson*, 2005]. Further analysis of how ultrasonic velocities and amplitudes were affected by the increase in pressure can be found in Section 5.1.2.

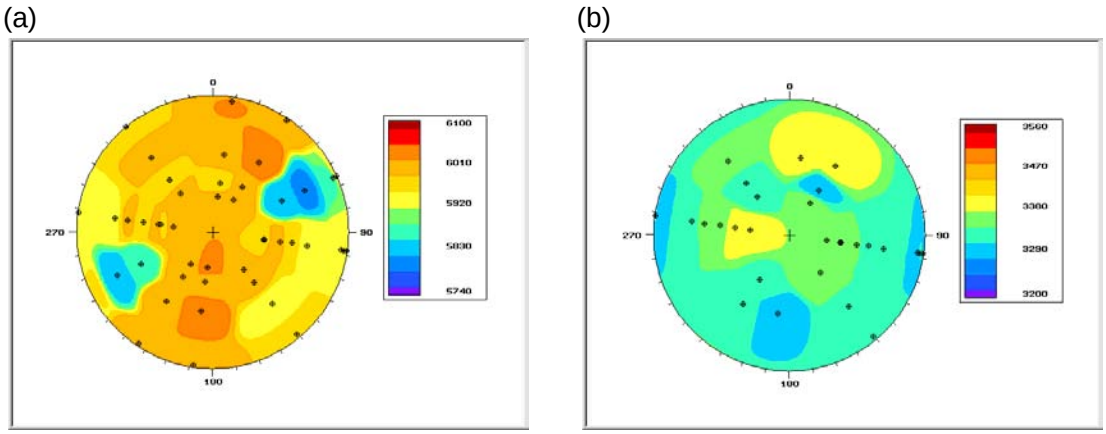

Figure 5-2: *Lower-hemisphere stereonets of a) P-wave velocity and b) S-wave velocity for the reference survey on 8th December 2004. The ray path orientations are shown by black markers.*

Figure 5-5 shows results of average P-and S-wave velocity and amplitude change. Amplitudes begins to increase immediately after heating of the canisters begins. There is a lag of approximately 10 days before velocity displays an increase. By 25th November 2004, P-wave velocity has increased by approximately 18m/s and S-wave velocity has increased by approximately 11m/s. For amplitudes, S-wave velocity shows a larger increase than P-wave velocity with a change of 10 and 7dB respectively. A significant increase for all four averages occurs around the end of November 2004. This rapid change is related to the change in pressure in the tunnel and deposition hole when the drainage was closed.

The measured changes in amplitude at the end of November 2004 are a reflection of a large increase in signal quality observed on the recorded waveforms. As described in Section 3.2.2 a cross-correlation algorithm has been used to measure changes in signal velocities through the monitoring period with an estimated uncertainty of approximately

±2m.s^{-1} between surveys. One of the assumptions in this method is that the character of the waveform does not change significantly. If the waveform shape being correlated does change then increased uncertainties can be produced in the velocity measurements. The sudden increase in signal quality has changed many of the signals sufficiently that cross correlation across this period is not possible with the reference survey of 20th March 2003 recorded at the start of monitoring. In order to produce the highest quality data analysis the ultrasonic survey data set has been split into two sections. An analysis of velocity changes during the heating period up to December 2004 (reported in Section 5.1.2) has used the reference survey at the start of monitoring. An analysis of velocity changes during the pressure increase (reported in Section 5.1.3) has used a different reference survey from 8th December 2004.

Using the reference survey of 8th December 2004, all waveforms have also been manually checked to assess whether cross-correlation can be used throughout the entire monitoring period from March 2003. Table 5-1 lists the raypaths for which P- and S-waves can be processed for velocity changes over the entire period. Table 5-2 and Table 5-3 gives similar information using two different reference surveys for the heating and pressure change phases respectively. Comparison of the three tables highlights the significantly greater amount of velocity data obtainable using the two separate surveys. All data from these ray paths are contained on an accompanying CD.

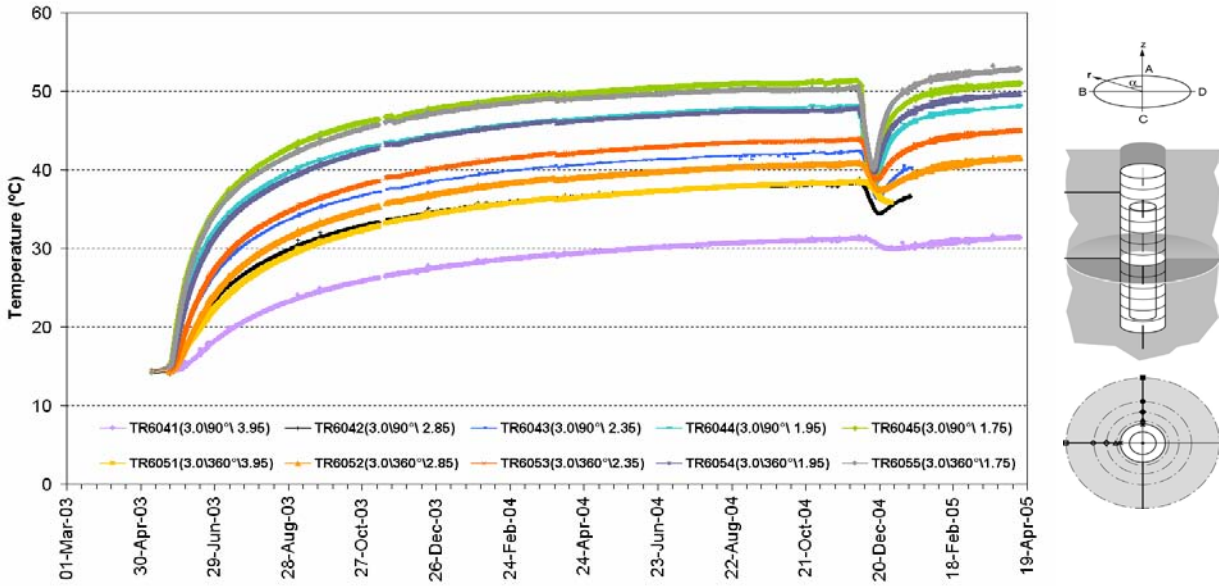

Figure 5-3: *Temperature around deposition hole DA3545G01. The sensors are positioned mid-way up the deposition hole with different depths into the rock mass (see right-hand inset).*

Using the calculations described in Section 3.2.2, results for Young's Modulus, Poisson's Ratio, Crack Density and Saturation parameters have been determined for the average P- and S-wave velocity (Figure 5-6). An increase in Young's Modulus occurs during heating of the canisters and measured Crack Density is observed to reduce. These effects are a result of induced thermal stresses causing pore spaces and microfractures to close up and increase the overall stiffness of the rock. Heating is occurring throughout the whole of the deposition hole. Combined with the surrounding

stress conditions and the complex tunnel-deposition-hole geometry, this means that regions around the deposition hole will be affected by heating in different ways. Modelling of the elastic thermal stresses could be employed to further interpret the obtained data. This is in agreement with the results obtained during the heating phase of the Tunnel Sealing Experiment at the URL, Canada [*Collins et al*., 2003].

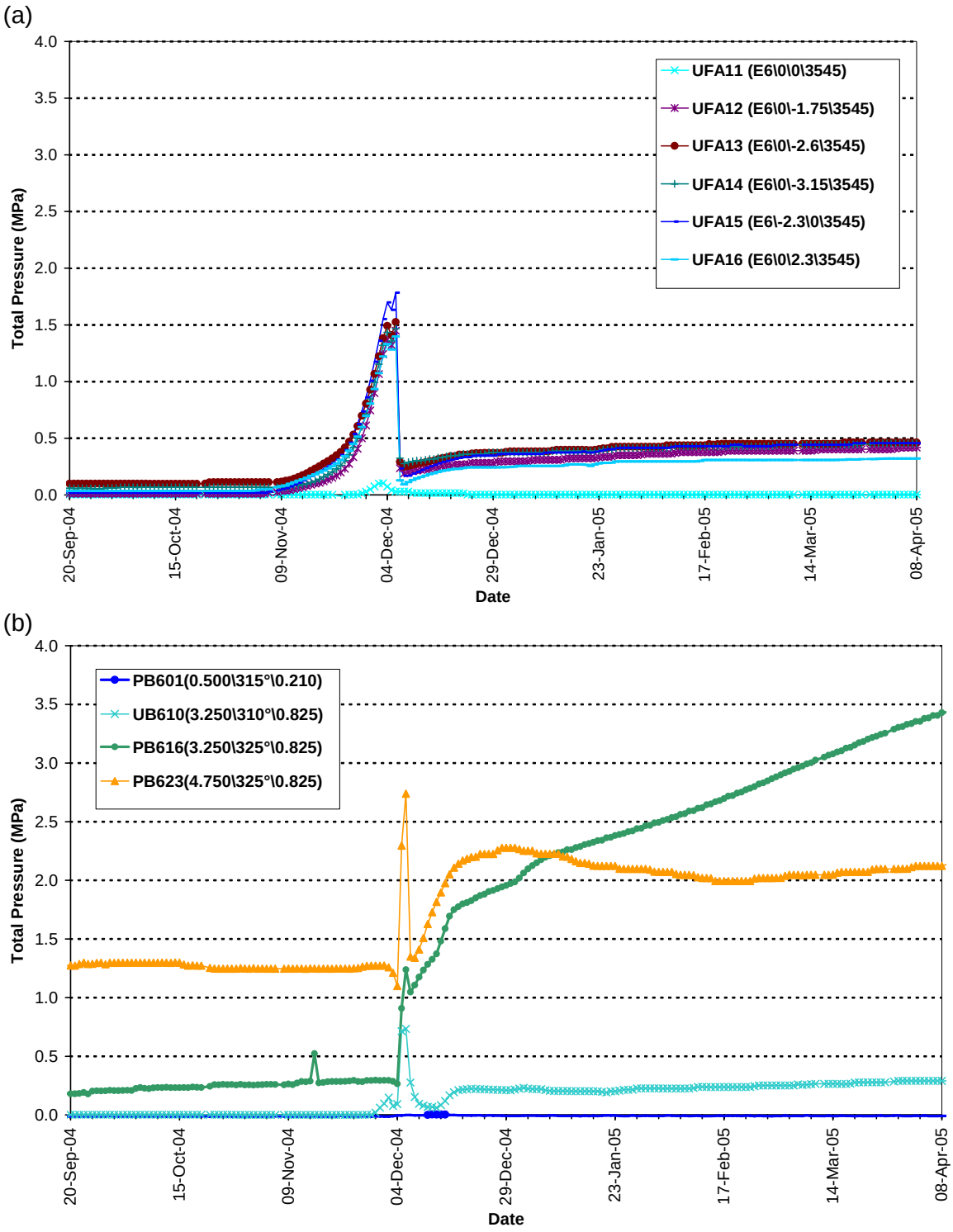

Figure 5-4: *Total pressure in (a) the backfill over deposition hole DA3545G01; and (b) in the rock adjacent to deposition hole DA3545G01.*

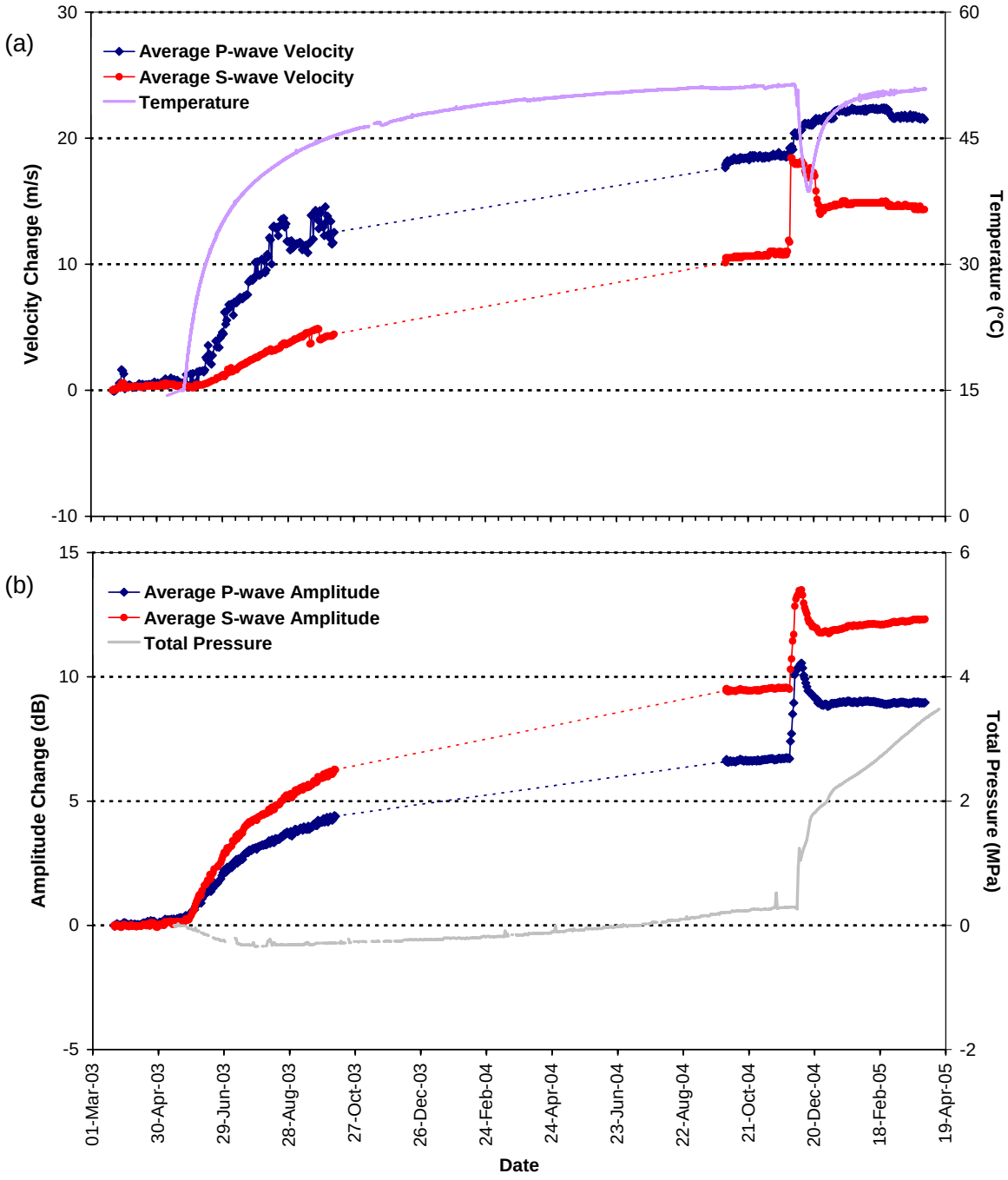

Figure 5-5: *Average P- and S-wave (a) velocity change, and (b) amplitude change, for the reporting period. Temperature (TR6045) and total pressure (PB616) are displayed on the secondary axes.*

Table 5-1: Raypaths for which P- and S-wave velocity changes are possible over the entire monitoring period, using the reference survey on 8th December 2004,

	Transmitter #							
Receiver	***1***	***2***	***3***	***4***	***5***	***6***	***7***	***8***
1			V_P				V_P	V_P
2			V_P				V_P	V_P
3			V_P, V_S			V_P	V_P	V_P
4				V_P		V_P		V_P
5	V_P							
6	V_S				V_S			
7		V_P				V_P		V_P
8		V_P			V_S	V_P		V_P
9								
10			V_P	V_P				V_P
11				V_P				V_P
12		V_P		V_P, V_S				V_P
13	V_P	V_S						
14	V_P	V_P				V_P		
15	V_P	V_P				V_P		
16		V_P		V_P, V_S		V_P		

Table 5-2: Raypaths for which P- and S-wave velocity changes are possible over the heating phase, using the reference survey on 20th March 2003,

	Transmitter #							
Receiver	***1***	***2***	***3***	***4***	***5***	***6***	***7***	***8***
1			V_P				V_P, V_S	V_P, V_S
2			V_P	V_P			V_P	V_P
3			V_P, V_S	V_P		V_P	V_P	V_P, V_S
4				V_P		V_P	V_P	V_P, V_S
5	V_P				V_P	V_P	V_P	
6	V_P, V_S	V_P				V_P	V_P	
7	V_P	V_P, V_S			V_P	V_P, V_S	V_P	V_P
8		V_P			V_P	V_P, V_S	V_P	V_P, V_S
9								
10		V_P	V_P	V_P			V_P	V_P
11			V_P	V_P, V_S			V_P	V_P
12		V_P		V_P, V_S			V_P	V_P, V_S
13	V_P, V_S	V_P, V_S	V_P	V_P, V_S	V_P	V_P		
14	V_P, V_S	V_P, V_S	V_P, V_S	V_P	V_P	V_P		
15	V_P, V_S	V_P	V_P, V_S	V_P		V_P, V_S		
16	V_P, V_S	V_P		V_P, V_S		V_P		

Table 5-3: Raypaths for which P- and S-wave velocity changes are possible over the pressure change phase, using the reference survey on 8th December 2004.

	Transmitter #							
Receiver	***1***	***2***	***3***	***4***	***5***	***6***	***7***	***8***
1			V_P	V_P	V_P		V_P, V_S	V_P
2			V_P	V_P, V_S	V_P	V_P	V_P, V_S	V_P, V_S
3				V_P	V_P	V_P	V_P, V_S	V_P
4			V_P	V_P	V_P	V_P	V_P	V_P
5	V_P	V_S			V_P, V_S	V_P, V_S	V_P, V_S	V_S
6		V_S				V_S	V_S	V_S
7	V_P, V_S	V_P, V_S			V_P	V_P, V_S	V_P	V_P
8		V_P			V_P, V_S	V_P, V_S	V_P	V_P
9								
10		V_P	V_P	V_P, V_S			V_P	V_P
11		V_P	V_P	V_P, V_S			V_P	V_P
12		V_P	V_P	V_P, V_S				V_P
13	V_P, V_S	V_P, V_S	V_P	V_P, V_S	V_P	V_P		
14	V_P, V_S	V_P	V_P, V_S	V_P	V_P, V_S	V_P		
15	V_P, V_S	V_P	V_P	V_P	V_P	V_P, V_S		
16	V_P	V_P	V_P	V_P, V_S	V_P	V_P		

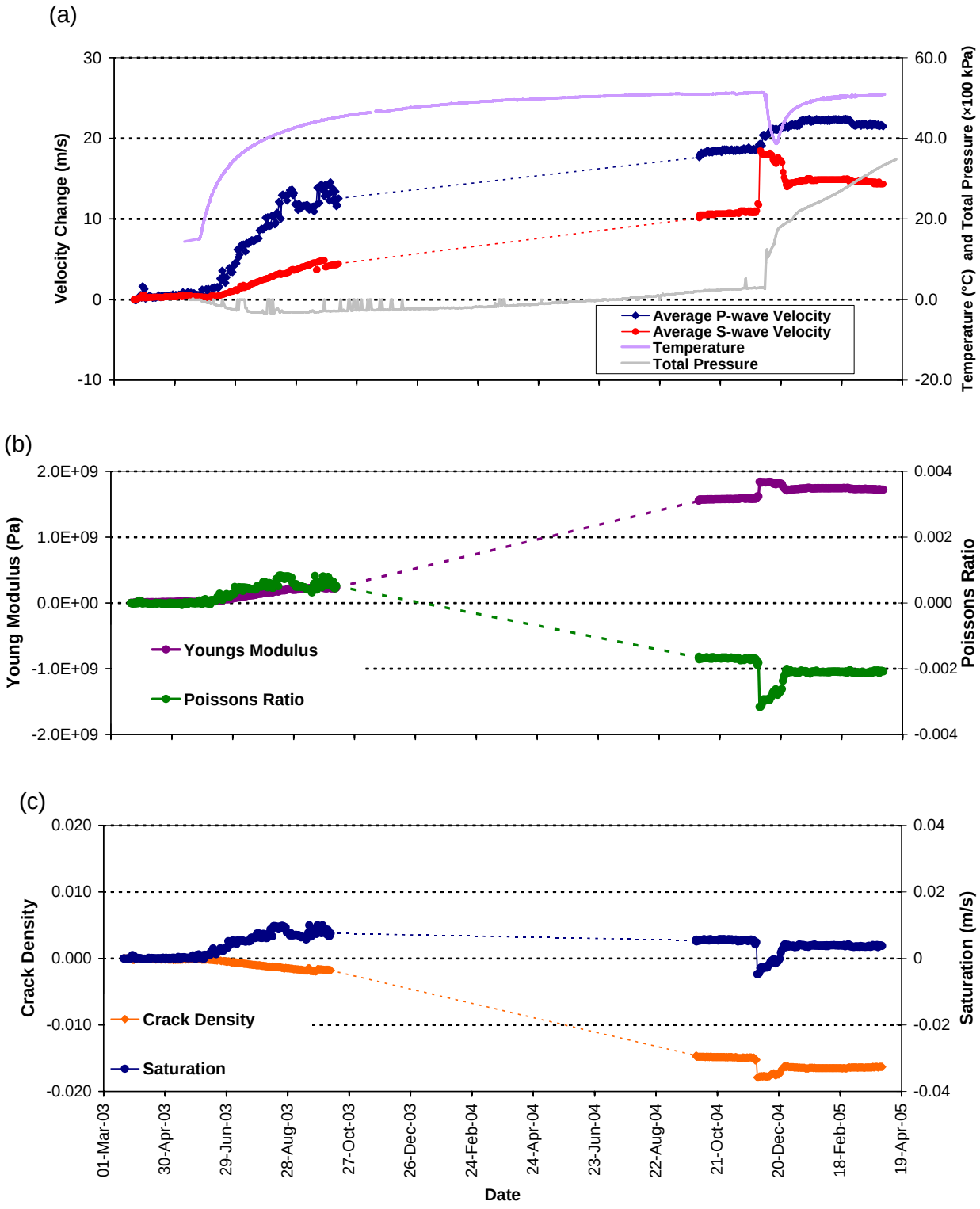

Figure 5-6: *Modulus changes for average velocity over the reporting period. (a) shows the average P- and S-wave velocity change with temperature and pressure measurements from deposition hole DA3545G01, (b) shows the Young's Modulus and Poisson Ratio, (c) shows the crack density and saturation.*

5.1.2 Response to Heating

Velocity and amplitude changes observed during the ultrasonic surveys for the period 20th March 2003 to 25th November 2004 are described here. This period relates to a significant change in temperature in the rock mass as a response to the heating of canisters in the deposition holes. Velocity and amplitude changes measured after this period are presented in the following section. Velocity changes are measured between transmitter-receiver pairs using a cross-correlation technique that allows a velocity resolution of ±2m.s^{-1} (Section 3.2.2). The first survey on 20th March 2003 is used as the reference survey.

Pettitt et al.[1999a] categorised the raypaths from the ultrasonic surveys into six types depending on their orientation with respect to the deposition hole. The ray paths are shown in Figure 5-7 along with an interpretation of the ultrasonic results from the excavation phase of the experiment in terms of disturbed and damaged regions around the excavation void.

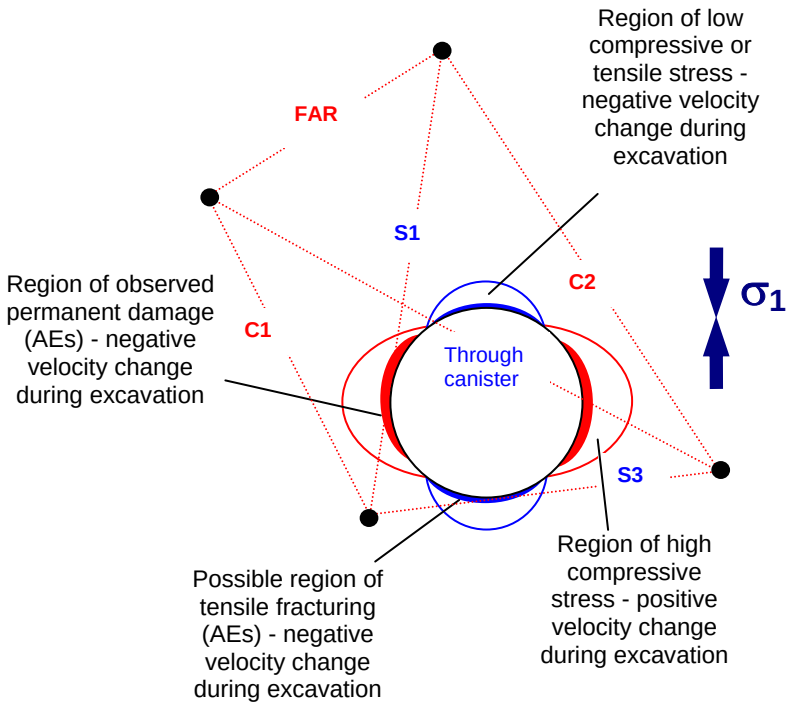

Figure 5-7: *Interpretation of the ultrasonic results during excavation in terms of disturbed and damaged regions around the deposition hole. Zones of induced stress are inferred from elastic modelling and the σ_1 orientation. After Pettitt et al.,[1999a].*

Figure 5-8 displays velocity results for raypaths in the 'S3' category, as described in Figure 5-7. These raypaths pass within centimetres of the deposition hole through the excavation damage zone, in a region of low compressive or tensile stress. The plot also shows how velocity changes vary down the deposition hole. The three raypaths closest to the bottom of the deposition hole show increases in velocity, which coincide with the start of heating and which then follow the trend in temperature change. The greatest P-wave velocity increase of approximately 40m.s^{-1} occurs between transmitter 1 and receiver 6. An S-wave is also present on this raypath, showing an increase of 15m.s^{-1}. The top raypath, closest to the tunnel, shows little variation in velocity. This could be due to lower temperatures in the rock nearer the tunnel and above the canister location (between 449 and 451m depth).

Figure 5-9 shows velocity results for raypath category ‘S1’. In this instance, raypaths pass through a region of high compressive stresses and permanent damage close to the tunnel wall observed by relatively high AE activity during excavation. Heating of the canister does not produce the same response as observed on ray path category ‘S3’ with a lower correlation between the trends in velocity and temperature. Over time all transmitter receiver pairs demonstrate a constant increase in velocity, of between 15 and 40 m/s, however the short-term response to heating is less responsive. Only transmitter 7 to receiver 7 displays a rapid change; a decrease of 15 m/s.

The majority of processed raypaths show similar behaviour. A minority exhibit higher complexity and sometimes decreases in velocity. This may be due to the different stress disturbed and/or damaged regions through which the ray paths travel. *Pettitt et al.*[1999a] observed systematic differences in ray path velocity during the deposition hole excavation and related these to changes in the stress distribution and recorded AEs. Heating applies a thermal stress to the rock mass around the deposition hole which interferes with the stresses induced by excavation of the deposition hole. The increase in observed velocity and amplitude values is due to closure of microcracks and pore spaces in the damaged zone and surrounding rock indicating that the thermal stresses are acting to increase the compressive stresses around the deposition hole. S-waves exhibit a similar behaviour to the P-waves, albeit with a generally lower velocity change. An example of this difference is between transmitter 1 and receiver 6 in Figure 5-8 where both P and S wave velocities have been obtained.

When unconfined rock samples are heated in a laboratory environment thermal expansion of the sample causes tensile stresses leading to an opening of existing microcracks. In the case of the Prototype Repository, the rock around the deposition hole is confined by the *in situ* stresses and the bentonite buffer filling the tunnel and deposition hole. Expansion of the rock fabric cannot therefore act outwards and can only lead to compressive stresses acting on the existing microfractures and pore spaces in a symmetric pattern around the canister deposition hole. This effect will be reduced close to the deposition-hole wall where confinement stresses are reduced to that produced by the bentonite buffer. The response can be investigated further through the examination of thermal numerical models and laboratory experiments on confined rock samples.

Figure 5-10 and Figure 5-11 compare the results of average velocity and amplitude changes across the different raypath categories described in Figure 5-7. All ray path categories show an overall increase in velocity during the heating period, however their temporal response differs. ‘S3’ raypaths, passing through a low compressive or tensile region, show the largest overall increase in velocity, increasing by over 25m/s for P-wave and 10m/s for S-wave by the end of this phase of heating. Raypaths that pass through compressive zones exhibit much less average increase (categories ‘S1’, ‘C1’, ‘C2’); ‘S1’ raypaths exhibit approximately half of the average P-wave velocity change observed on ‘S3’. On all categories other than ‘S3’ an initial drop in P-wave velocity is observed during the first few months of heating. S-wave velocities on all categories show a very similar pattern except that the S-wave velocities on ‘S3’ raypaths respond to heating much quicker. The initial drop in P-wave velocity is not observed on the S-waves. S-wave velocities do not respond to fluids so it can be inferred that the fall in P-wave velocities for ray paths passing through compressive zones is due to a de-saturation of the rock mass. This is discussed further below. The P- and S-wave amplitudes all show very similar patterns of increase over time although there is some variation in the magnitudes of change overall. S-wave amplitudes generally show the larger increases.

A different response to heating has been shown for velocities along ray path categories 'S3' and 'S1'. These two ray path categories pass through volumes of the rock mass experiencing opposite induced-stress regimes. The 'S3' category passes through a volume that is unloaded and hence experiences low compressive stress (depending on the *in situ* σ_1 to σ_3 ratio volumes close to the deposition hole wall may experience tensile stresses). The 'S1' category passes through a volume experiencing increased compressive stresses (*Pettitt et al.*[2000] shows modelled induced stresses from excavation alone to be of the order 100MPa). Similarly, categories 'C1', 'C2' and 'Far' pass through compressive zones. The low-compressive, unloaded, region appears to be more responsive to heating in the short term, exhibiting rapid increases in P- and S-wave velocity. The compressive zone responds similarly in the long term, exhibiting increases in velocity, but both P and S-wave velocities respond slower in the first few months of heating. Figure 5-12 shows changes in Young's Modulus, Poisson's Ratio, Crack Density and Saturation parameters for the ray path categories calculated from the average measured velocities. The faster response to heating on the 'S3' category is observed in the increase in Young's modulus (indicating a stiffer rock mass) and the decrease in Crack Density. The difference in the rate of response between the two raypath categories is interpreted as a different magnitude of response of the microfractures to increasing thermal stresses. In the low-compressive region, existing microfractures will initially be unloaded and hence more open than similar microfractures in the compressive region, where stresses act to clamp the fractures (i.e. the absolute Crack Density will be less). As thermal stresses are applied to the rock mass the open fractures will be far more sensitive to the stress increase and hence respond to a far greater extent, and far quicker, than those that are pre-clamped, resulting in more responsive ultrasonic signals. The compressive stresses will be variable with orientation and distance from the deposition hole, and hence may explain small differences recorded on individual ray paths.

Another effect is superimposed onto the rock's response to thermal stresses. This is measured as a reduction in P-wave velocities compared to S-wave velocities in the first few months of heating. Figure 5-12d shows the calculated change in 'Saturation' of the rock mass using the method of *Zimmerman and King*[1985], as described in Section 3.2.2. A de-saturation occurs on all raypath categories, other than 'S3', during the first period of monitoring. This must be caused by a drying of the rock mass, in the zones experiencing high compressive stresses, as heat is applied to the rock (i.e. both pressure and temperature are acting to expel moisture). In the low-compressed, or tensile, region sampled by raypath category 'S3', Saturation increases during this period. This is probably caused by hot fluids expanding into the open microfracture fabric.

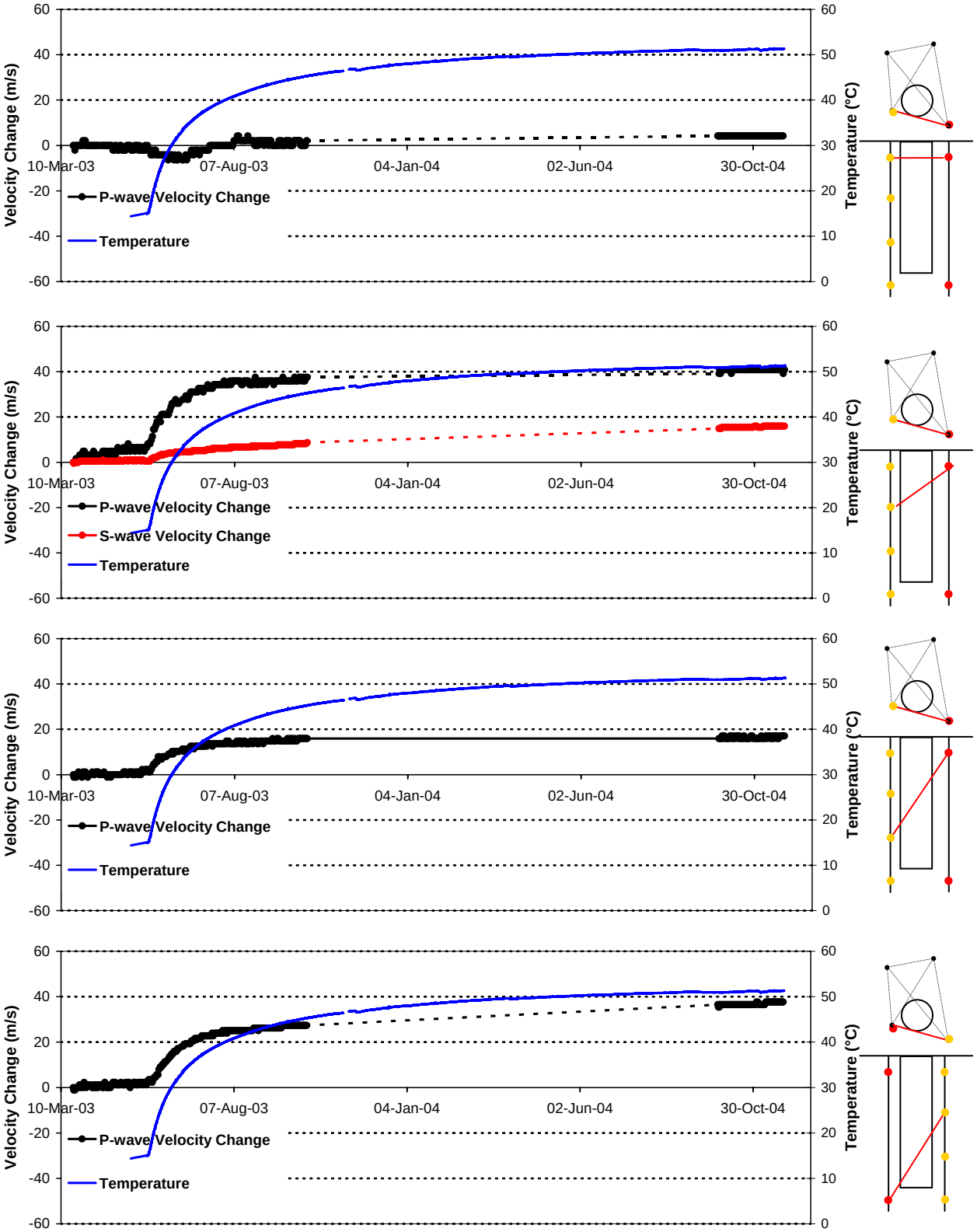

Figure 5-8: *Velocity changes measured on ray path category 'S3' (Figure) for deposition hole DA3545G01. Ray paths shown are from a* top *transmitter to receivers with increasing depth: a) transmitter, t_n=1, receiver, r_n=5; b) t_n=1, r_n=6; c) t_n=1, r_n=7; d) t_n=4, r_n=2. Schematic diagrams in the right margin indicate the relative locations of transmitter (red) and receiver (gold). The red arrow indicates the passing depth. Temperature (TR6045) is displayed on the secondary axes.*

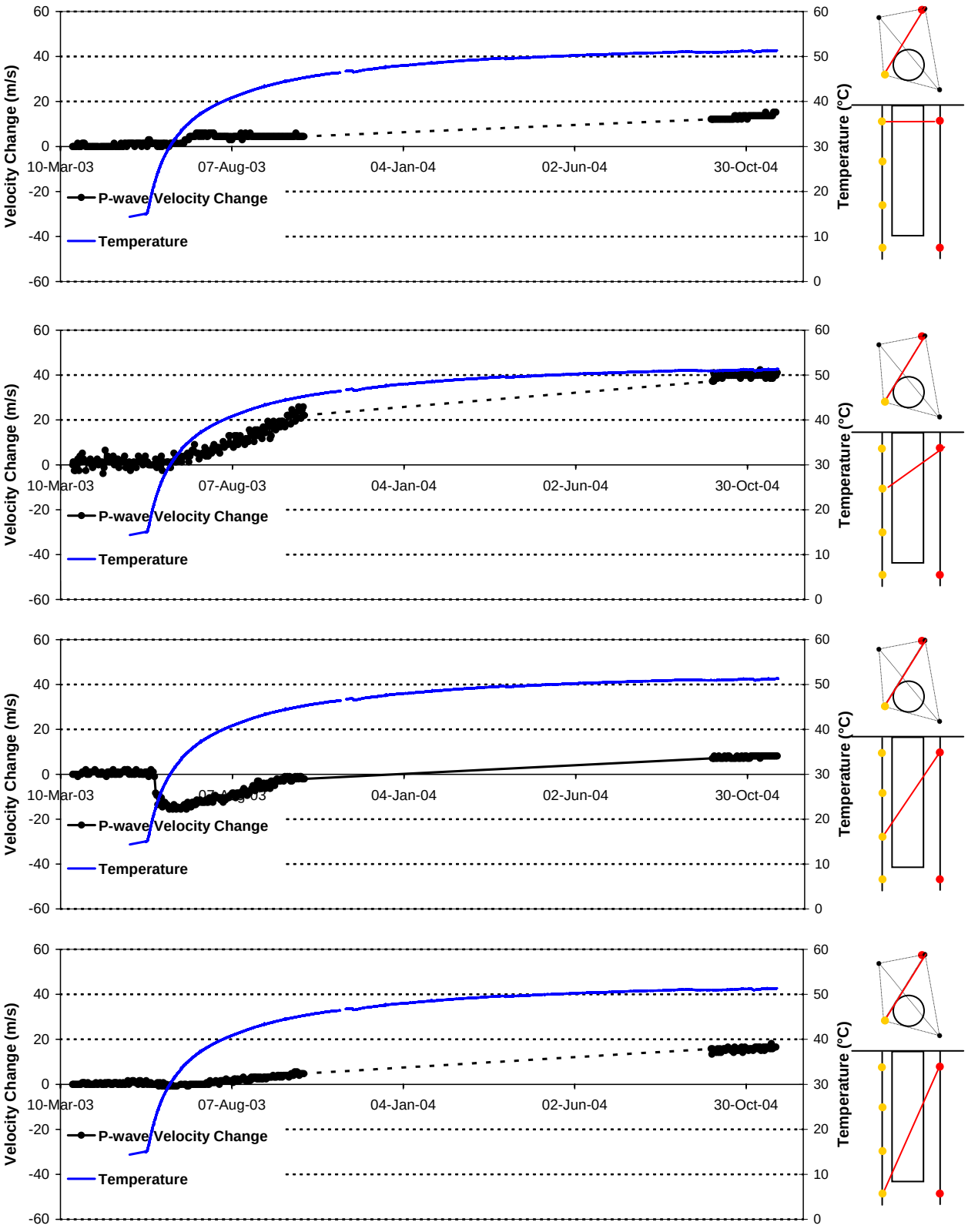

Figure 5-9: *Velocity changes measured on ray path category 'S1' (Figure 5-7) for deposition hole DA3545G01. Ray paths shown are from a top transmitter to receivers with increasing depth: a) transmitter, t_n=7, receiver, r_n=5; b) t_n7, r_n=6; c) t_n=7, r_n=7; d) t_n=7, r_n=8. Schematic diagrams in the right margin indicate the relative locations of transmitter (red) and receiver (gold). The red arrow indicates the passing depth. Temperature (TR6045) is displayed on the secondary axes.*

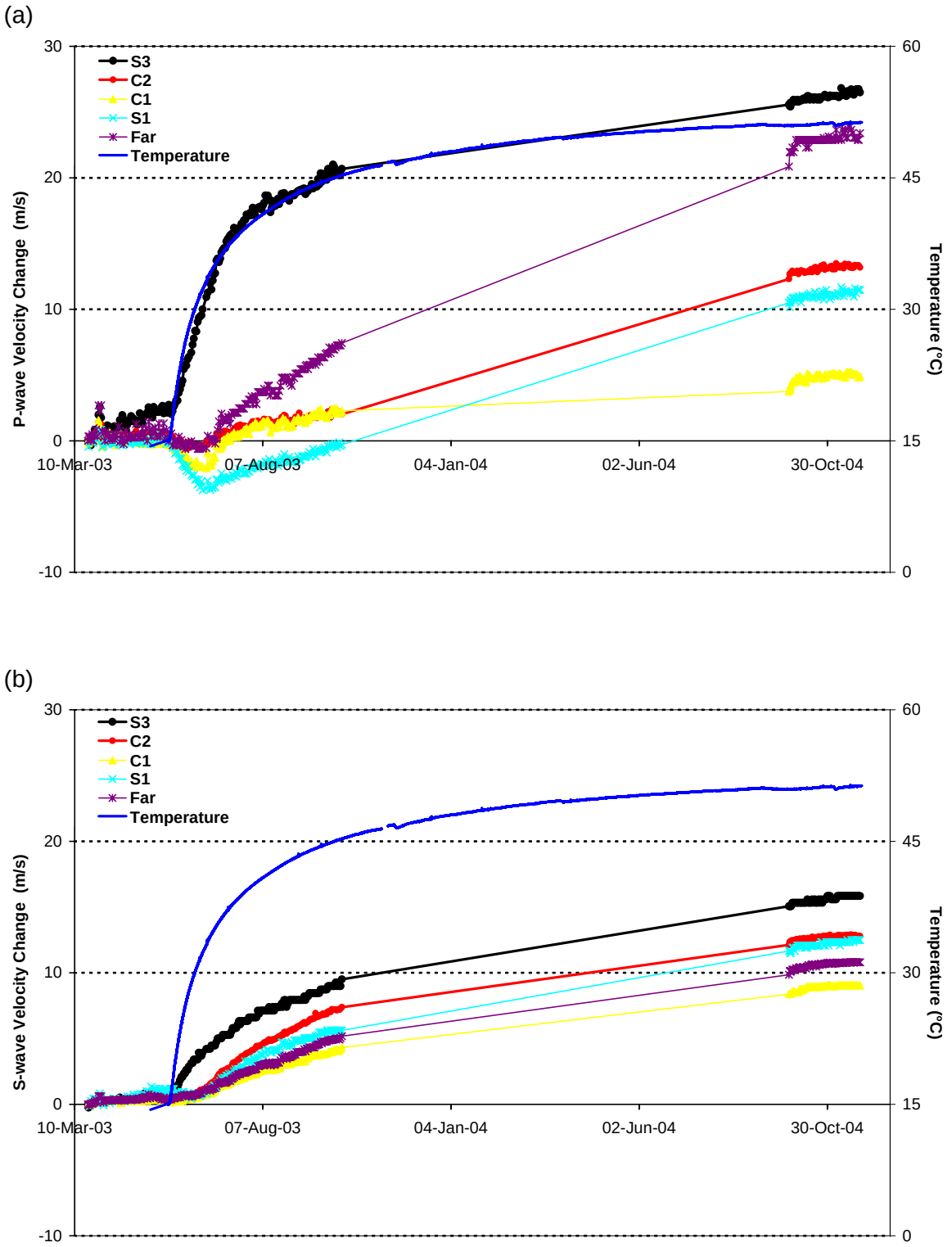

Figure 5-10: *Velocity change plots of 5 raypath categories around deposition hole DA3545G01 for (a) P-waves and (b) S-waves. Temperature (TR6045) is displayed on the secondary axes.*

(a)

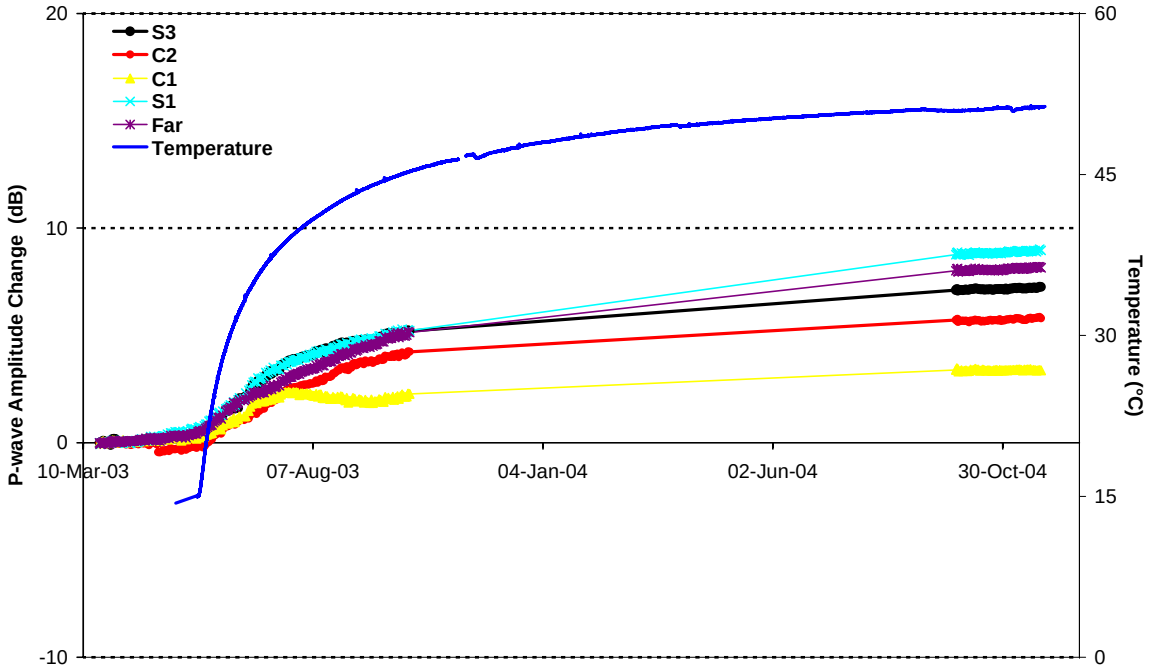

(b)

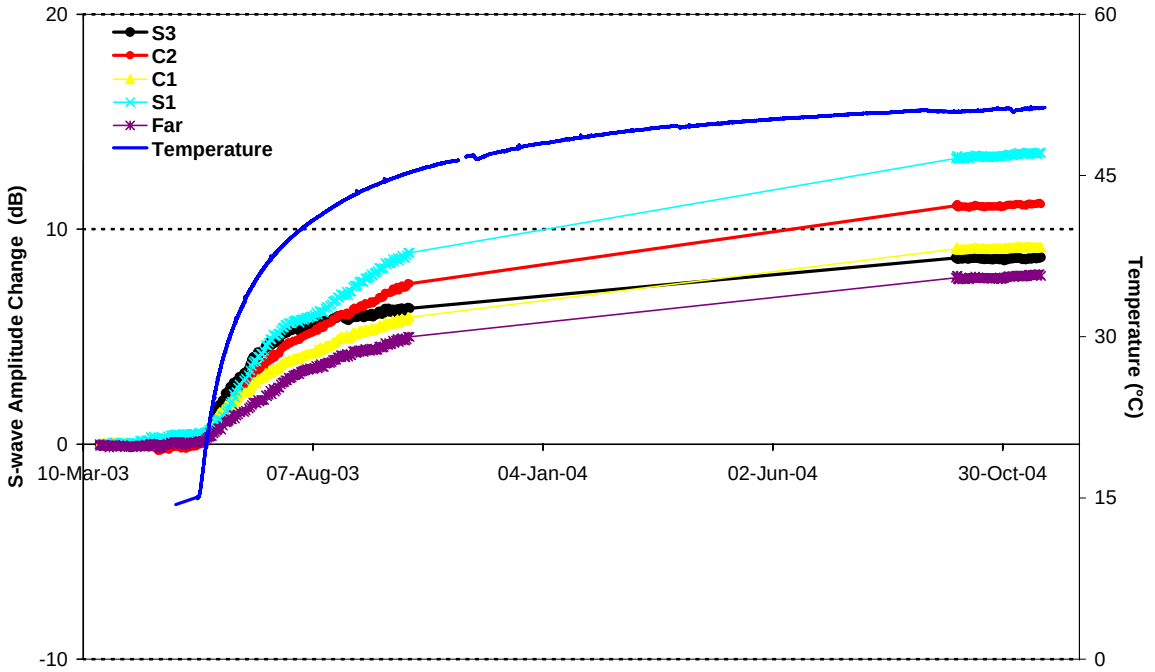

Figure 5-11: *Amplitude change plots of 5 raypath categories around deposition hole DA3545G01 for (a) P-waves and (b) S-waves. Temperature (TR6045) is displayed on the secondary axes.*

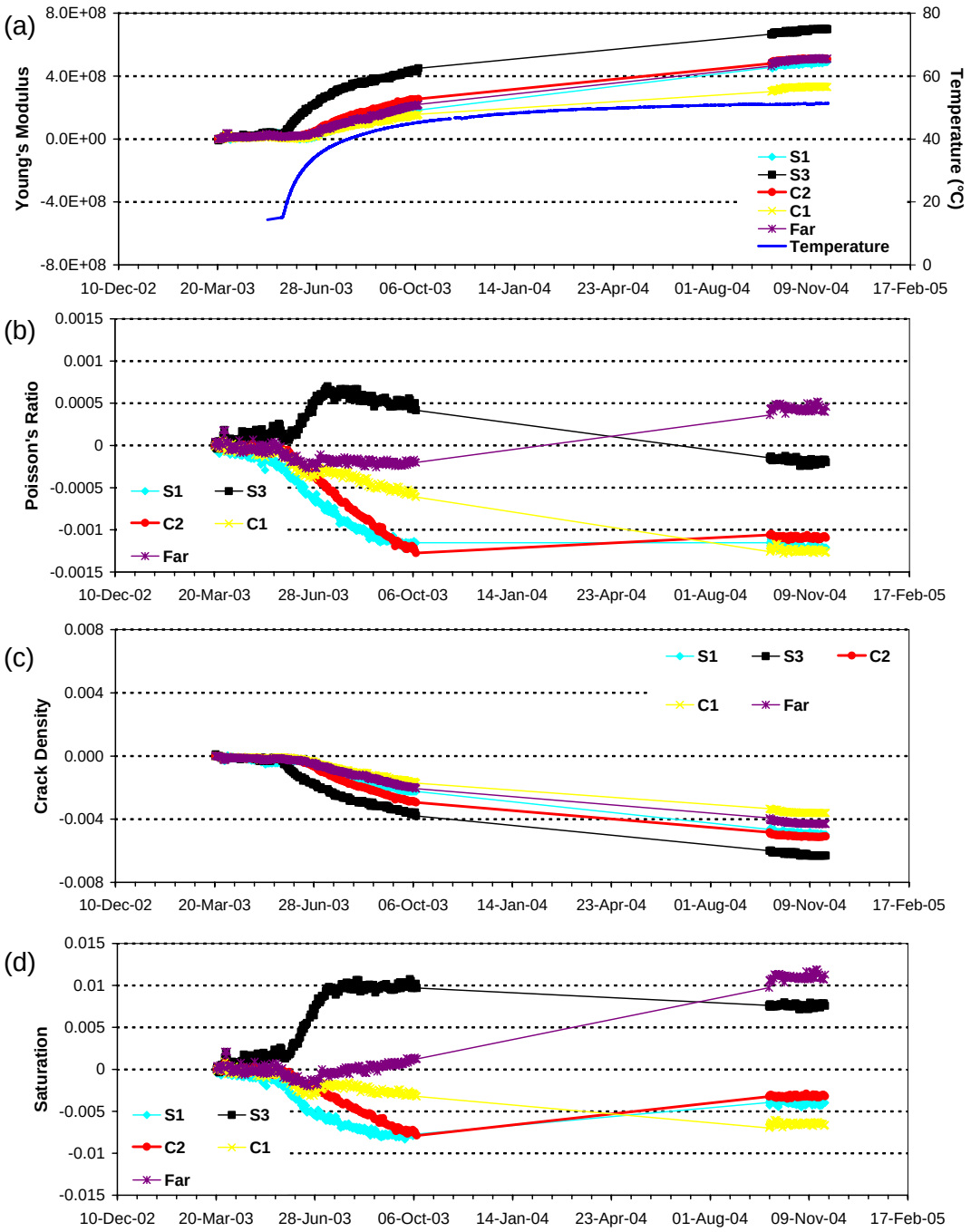

Figure 5-12: *Modulus during heating phase for average P- and S-wave velocity values on different raypath orientations. (a) Young's Modulus, (b) Poisson's Ratio, (c) Crack Density and (d) Saturation. Raypath orientations are described in Figure .*

5.1.3 Response to Drainage Closure

As described in the previous sections, processing of ultrasonic surveys during drainage closure has used a different reference survey to that used in the previous section. This is due to the significant increases in signal amplitudes recorded at the end of November 2004 as a response to increases of pressure in the tunnel. The change in reference survey provides a greater accuracy in the measured velocity changes, and increases the number of ray paths that can be used during this period compared to using the original reference survey. In this section we therefore show results from velocity changes through the second monitoring period using a reference survey undertaken on 8th December 2004 when signal qualities were at their highest.

The following important events occur in and around deposition hole DA3545G01 during this period [*Johannesson*, 2005]:

- The drainage of the Prototype Repository was closed on 1st November 2005.
- The power to all the canisters in the Prototype Repository was switched off on 2nd December 2005 due to electrical problems with the heaters.
- Damage was observed on 6th December 2005 on canister number 6 (deposition hole DA3545G01).
- The drainage of the tunnel was opened on 6th December 2005.
- The power was switched on to all the canisters in the Prototype Repository (except canister number 2) on 15th December 2005.

During November 2004, drainage in the Prototype tunnel was closed causing pressure to build up rapidly in the backfill of the tunnel [*Johannesson*, 2005]. An increase was observed in the total pressure in the backfill of the tunnel and on the side wall adjacent to the buffer in the deposition hole (Figure 5-4). The rapid increase in pressure in the deposition hole occurred over only a few days (between 4th December and 6th December) and resulted in significant changes to the character of many recorded waveforms. An example demonstrating the extent of this change is presented in Figure 5-13. The amplitude of raypath P1_R6 increases by over 3 times over a single day (29th November 2004). This suggests that as pressure is increased in the rock surrounding the deposition hole, attenuation of the ultrasonic waves is reduced meaning that they can pass more efficiently through the rock medium. The reduction in attenuation is either a result of an increase in saturation in the rock mass (fluids are pushed into microcracks and pore spaces), or a result of a reduction in crack density caused by a closing of pre-existing microcracks, or a combination of the two. Note that the example amplitude change occurs 5-6 days *before* the pressure change is recorded inside the deposition hole.

A correlation is observed between the date on which the rapid changes in velocity and amplitude occur and the depth of the raypaths down the deposition hole. Figure 5-14 shows velocity and amplitude change plots for ray paths along category ‘S3’ (as described in the previous section) that pass through the low compressive stress, or tensile, zone. The four raypaths have been chosen because they pass at increasing depths down the deposition hole. Velocity increase commences on the raypath nearest the tunnel, Transmitter 1 to Receiver 5, on 26th November 2004. The next raypath to show change in velocity is Transmitter 1 to Receiver 7 on 30th November 2004. The lower two raypaths both show slight changes on 1st December 2004. A similar pattern of

change is observed for the P- and S-wave amplitude data. It should be noted that changes occur on raypaths from the same transmitter at different times indicating this effect is not a response associated with sensor coupling to the instrumentation boreholes, but must be a response of the rock mass. Transient changes in the amplitudes and velocities are observed on some ray paths after 6th December. These changes result from variations in temperature and pressure following switching off of the heaters and re-opening of the drainage.

Figure 5-15 has the same configuration down the deposition hole, but along raypath category 'S1', which passes through the high compressive stress zone. Little velocity change is observed for two of the raypaths. Amplitude results agree with the observations made above that changes occur earlier for ray paths nearest the tunnel (at lower depths), i.e. Transmitter 3 to receiver 13 increases after 27th November 2004, whereas Transmitter 8 to Receiver 8 increases after 1st December 2004. This change is observed at the same time for both P- and S-wave amplitudes.

The same is also true for velocity and amplitude measurements shown in Figure 5-16. These are along raypath category C2 that does not skim the deposition hole, but also passes through regions of induced compressive stresses. Reductions in velocities and amplitudes are observed on some raypaths indicating that the pressure changes may be preferentially opening fractures in some cases.

The pressure measurements in Figure 5-4 show that pressure in the tunnel backfill above the deposition hole built up slowly starting at the closure of drainage in early November 2004, whereas pressure increases in the buffer inside the deposition hole occurred over a relatively short period of time (a few days). The highest magnitude changes in pressure inside the deposition hole occur nearest to the tunnel and they all occur at the same time (on or around 5th December). An interpretation of this response is that some form of event occurred on this date that suddenly allowed a transfer of pressure into the deposition hole from above. This interpretation is also borne out by observations that the canister itself is now damaged [*Johansson*, 2005], and by acoustic emission observations reported in the following section.

Figure 5-17 displays the results of modulus changes recorded between Transmitter 3 and Receiver 13. This represents a typical change in velocity experienced as a result of pressure changes in the deposition holes. On 27th November 2005 there is a significant increase in P-wave velocity of approximately 10m/s. Young's Modulus and Poisson Ratio increase representing a stiffening of the rock through which the raypath travels. Crack density displays a slight decrease whereas saturation increases significantly (caused by a very small S-wave change measured on this ray path).

The ultrasonic results presented in Figure 5-14, Figure 5-15 and Figure 5-16 show an abrupt change in velocities and amplitudes occurring over short periods of time. This is mirrored in the rapid increase in Young's modulus values. Significantly, all these changes precede the measurements of pressure made within the deposition hole. There is also a trend for raypaths travelling at greater distance from the tunnel, further down the deposition hole, to change velocity and amplitude at a later time (between 26th November and 1st December). This pattern does not appear in the pressure measurements recorded within the deposition hole. The modulus results show that the rock around the deposition hole generally stiffens and the crack density reduces prior to the recorded increase in pressure. Our interpretation of these results is that a pressure and/or fluid field migrated through the rock mass, initiated by pressure within the tunnel

reaching a critical value on 26th November (approximately 0.75MPa). A fluid 'front' may have used the existing macro-fracture network to propagate away from the tunnel. The pressure or fluid field reached the floor level of the deposition hole on 1st December, but did not ingress into the deposition hole itself sufficiently to cause a response on the instruments contained there until 5th December when a sudden event occurred; it may have been inhibited by the bentonite buffer material. The event may have been induced by a combination of the pressure increases around the deposition hole and a rapidly cooling canister (the heaters were switched off on 2nd December).

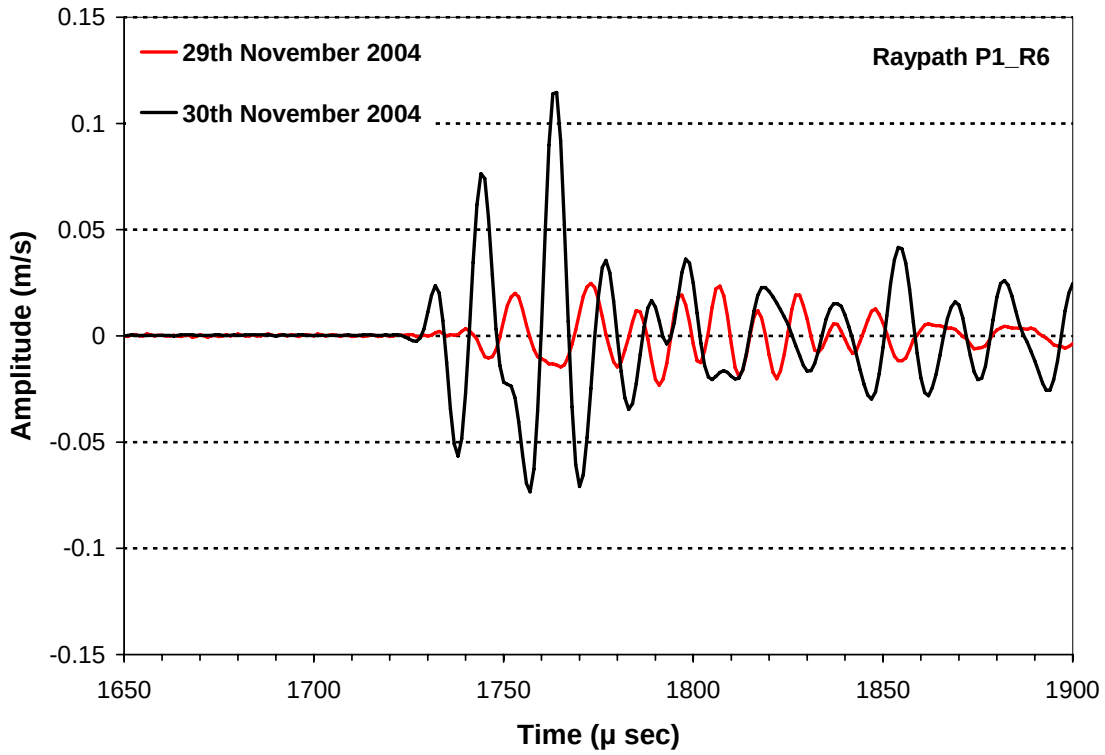

Figure 5-13: *Comparison between P-wave character of raypath P1_R6 on 29th November 2004 and 30th December 2004.*

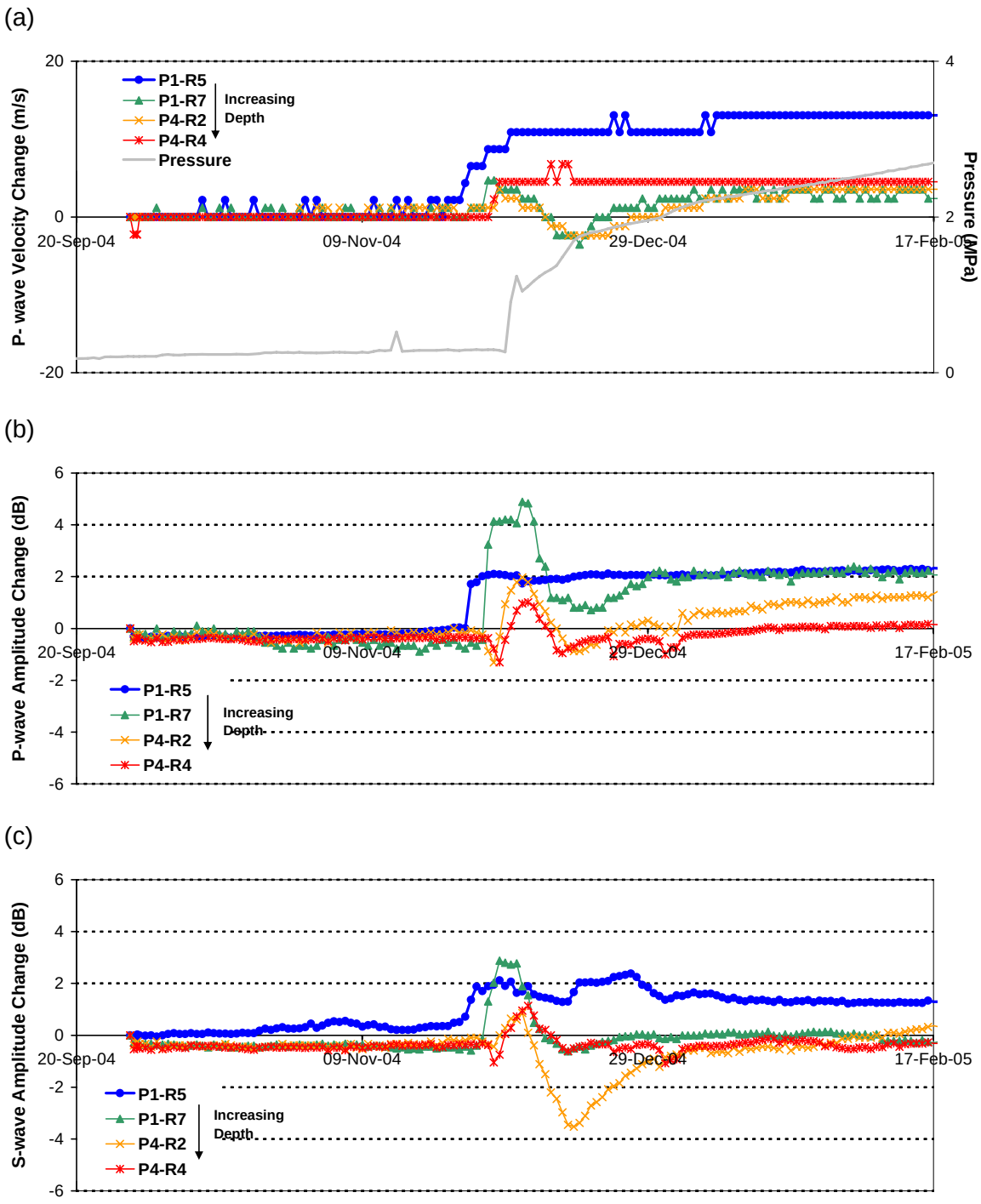

Figure 5-14: *(a) Velocity, (b) P-wave amplitude change, and (c) S-wave amplitude change for raypaths passing the deposition hole at varying depths but along the same orientation ('S3').Total pressure measured from instrument PB616.*

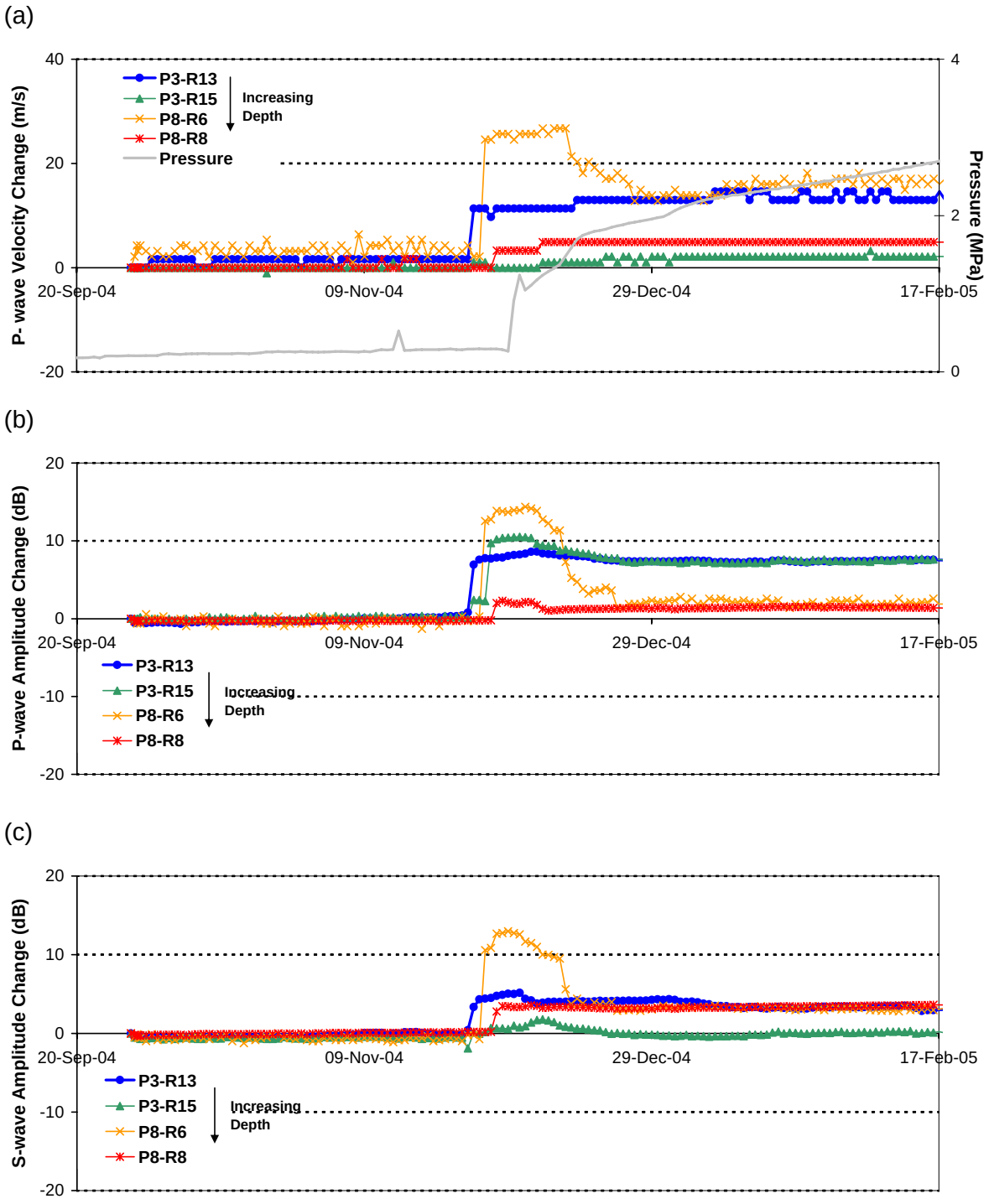

Figure 5-15: *(a) Velocity, (b) P-wave amplitude change, and (c) S-wave amplitude change for raypaths passing the deposition hole at varying depths but along the same orientation ('S1').Total pressure measured from instrument PB616.*

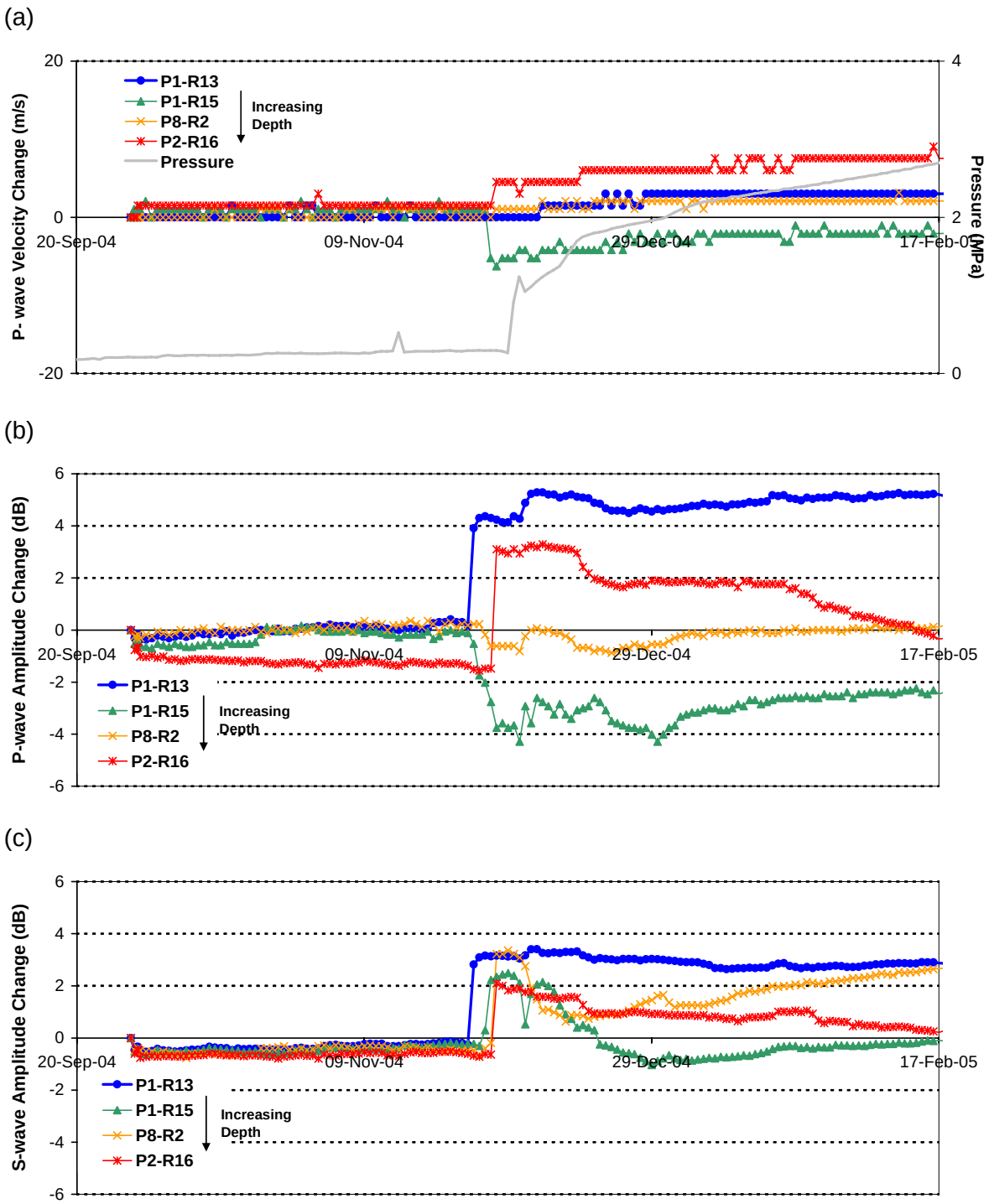

Figure 5-16: *(a) Velocity, (b) P-wave amplitude change, and (c) S-wave amplitude change for raypaths passing the deposition hole at varying depths but along the same orientation (at 60cm from deposition hole).Total pressure measured from instrument PB616.*

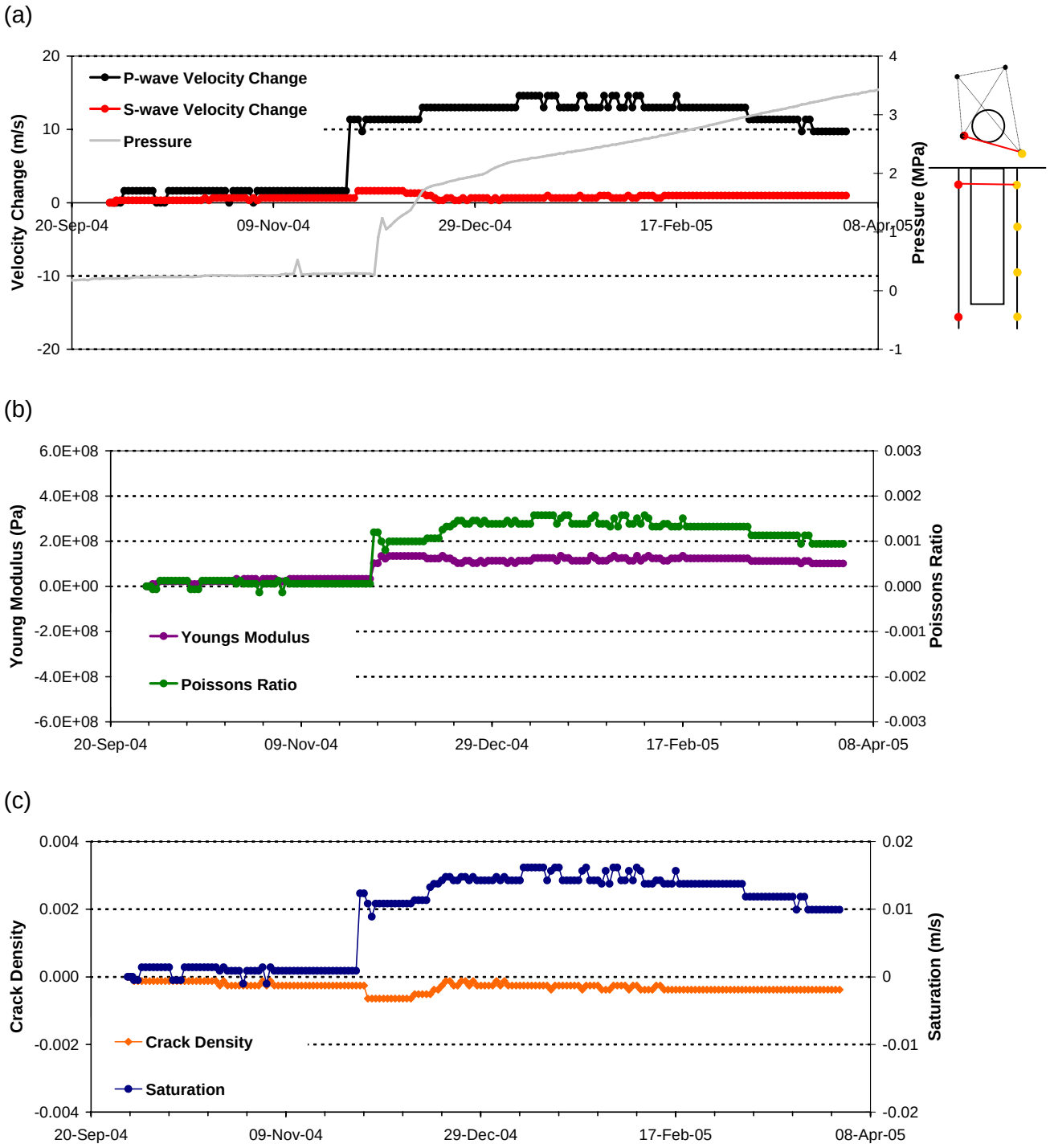

Figure 5-17: *Modulus changes for raypath from transmitter 3 to receiver 13. (a) shows the P- and S- wave velocity change, (b) shows the Young's Modulus and Poisson's Ratio, (c) shows the crack density and saturation.*

5.2 Acoustic Emissions

The processing procedure outlined in Section 3.2.2 has resulted in 219 events located with high confidence and with all events associated with noise having been removed. Estimated uncertainties on these events are of the order 10cm as described by calibration 'hits' performed within the deposition hole. Figure 5-18b shows the temporal response of the located AEs. An increase in activity occurs mid way through June, and peaks on 26th June 2003 when 13 events are located. Very few events are located in the volume during the three months preceding this date (two events occurred at the beginning of May). The start of activity coincides with the temperature reaching approximately 35^{o}C on the side wall of the deposition hole (Figure 5-18a). After monitoring recommences for the second period, few events are located except during the first half of December 2004. A peak of 23 located events on 5th December 2004 coincides with a period of change to total pressure and is discussed further below.

Figure 5-19 shows the location of all AEs located in the two monitoring periods from 20th March 2003. 73% of the events (160) are located around the walls of deposition hole DA3545G01 within the volume of the array. 48 events are also observed around the neighbouring deposition hole (DA3551G01) and in the floor of the tunnel in volumes outside of the array. The majority of the events around DA3545G01 locate close to the deposition hole wall, within the first 20cm. Waveforms of selected events are shown in Figure 5-20 to demonstrate the high quality data collected. Waveforms with low signals have ray paths that intersect the deposition hole volume and have been removed from the processing. In plan the majority of events are distributed in the NE and SW quadrants and coincide with regions of increased compressive stress as imaged during excavation [*Pettitt et al.*, 2000; *Pettitt et al.*, 2002]. Clusters of events are also observed in the NW and SE quadrants correlating to low compressive stress or tensile zones.

The AE activity is interpreted as stress disturbance of the rock mass, particularly around pre-existing macroscopic fractures that commonly intersect the excavation. The mechanism for producing the AEs could be associated with movement around the pre-existing macrofractures, or microcracking in the immediate vicinity of the fractures. As during deposition hole excavation some clustering of events in the sidewall is observed during heating, for example around 26th July, indicating that the disturbance is occurring in localised volumes (see clusters i and ii in Figure 5-19). It is concluded that the thermal-related activity is a re-initiation of the same stress-related processes that occurred during excavation, although with a much reduced intensity (884 events were located during the excavation monitoring).

The fact that the AE activity did not start immediately after heating began suggests that the thermal stresses had to reach a certain level before AEs were triggered. This could be a Kaiser-type effect, which takes place in rock and materials subjected to cyclic loading/unloading. In the Kaiser effect, the observed AE rate is zero or close to the background level so long as stress remains below the largest previously reached stress value [*Lavrov*, 2003]. In the case of deposition hole DA3545G01, the AE rate increases when it was excavated due to induced stresses that are high enough to create damage in weakened regions [*Pettitt et al.*, 1999a]. The AE rate only significantly increases again when the thermal stresses applied by heating the rock are greater than the peak ('memorised') stress during excavation, which occurs immediately behind the advancing face.

The peak rate of observed AE activity coincides with rapid changes in pressure in the Prototype Repository after fluid drainage was switched off on 1st November 2004. Figure 5-4 shows how total pressure (sum of the pore pressure and bentonite swelling pressure) in the backfill and rock around the deposition hole change during the second monitoring period. Total pressure in the backfill rises steadily for a month after the drainage is switched off. Total pressure in the rock remains reasonably constant during this time, but undergoes a rapid increase on the 4th and 5th December 2004. This results in 66 AE locations locating around deposition hole DA3545G01 between 25th November and 15th December.

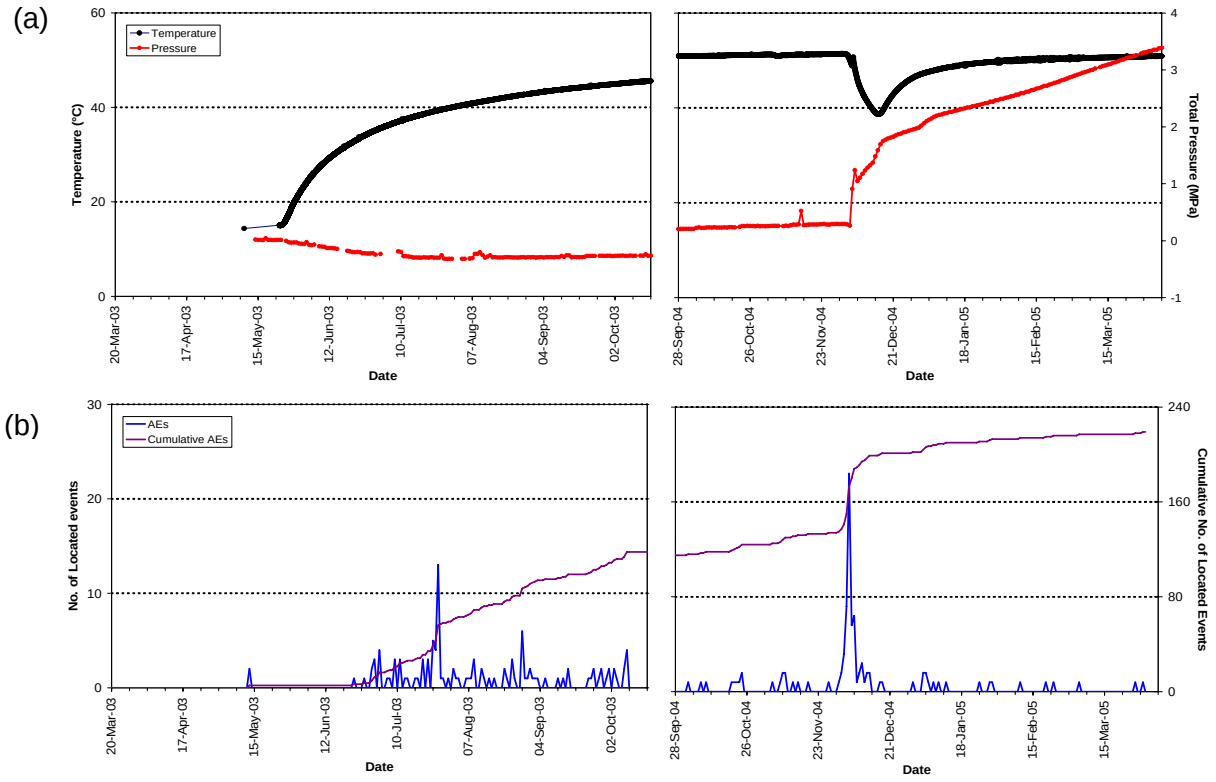

Figure 5-18: *Plots of (a) temperature and pressure, and (b) temporal response of AE activity Left hand plot is for the first period of monitoring performed in 2003. Right hand plot is for the second period of monitoring.*

Figure 5-21 shows in detail how the number of located AE events relate to pressure in the rock and buffer in this deposition hole. On 4th December 2004 there is a rapid increase in pressure, causing an increase in the number of located AEs. This is 35 days after drainage was switched off and coincides with damage to the canister [*Johannesson*, 2005]. A peak of 32 events occurs on 5th December 2005, when pressure in the buffer is highest. Figure 5-22B shows that acoustic emissions during this period locate predominantly around deposition hole DA3545G01. Two clusters have been identified during this time period (i and ii in Figure 5-22B). The increase in activity is therefore likely to be the result of stress changes in the rock around the deposition hole associated with this relatively sudden increase in pressure. The stress changes are inducing small scale movements on pre-existing microfractures, or are inducing new microfractures in weaker volumes of the rock. An increase in pore pressure may also assist in inducing slip on pre-existing microfractures, by reducing the normal stress on

the fractures. The peak in activity is only over a short time frame of only 2 days. However, AEs are still recorded 8 days afterwards. A cluster of events locates on the pillar side of the neighbouring deposition hole (DA3551G01) at approximately 4.7m depth during this period (Cluster iii in Figure 5-22C). These are likely to be created through the same mechanism.

Figure 5-23 shows the AEs are locating in similar distributions during this heating phase to those observed during excavation, and are hence controlled by the *in situ* stress field. AEs around DA3545G01 during this reporting period principally locate within the bounds of those that occurred during excavation and hence suggests they are created by movement on pre-existing fractures, but could also be a result of extension of microcracks already present or the formation of new microcracks in the existing damaged region.

Although the majority of the AEs locate close to the deposition holes, within the extent of activity observed during excavation, some disturbance in the rock mass between the deposition holes is also present. A total of 11 AEs have been located within the pillar volume and all occur at a similar depth below the tunnel (Figure 5-19), approximately 455.9m depth, and 1m above the floor of the deposition hole. They define an approximately horizontal planar feature. This level coincides with a semi-horizontal macroscopic fracture that is observed to intersect the deposition holes at this height [*Pettitt et al.*, 2000]. Three low-magnitude events were also observed along this fracture during the excavation phase [*Pettitt et al.*, 1999a].

During the 12 months of monitoring the heating phase of the Prototype Experiment, 219 AEs have been located. The events consist of two types: a) 115 events associated with an increase in temperature; b) 104 events associated with a relatively sudden pressure change. The amount of activity is relatively small compared to the excavation period (where 1153 events were located) and similar experiments where significant rock damage is observed (e.g. the Pillar Stability Experiment). This indicates that heating of the deposition hole canisters has not so far resulted in a significant creation of new micro-fractures or the disturbance of pre-existing fractures. The monitoring has shown that the rock is sensitive to sudden changes in conditions in the deposition-hole environment, such as the increase in pore pressure when drainage from the tunnel was closed off. This change in environmental conditions created a disturbance in the stress field around the deposition hole that was sufficient to cause a disturbance to the rock mass and was detected as AEs.

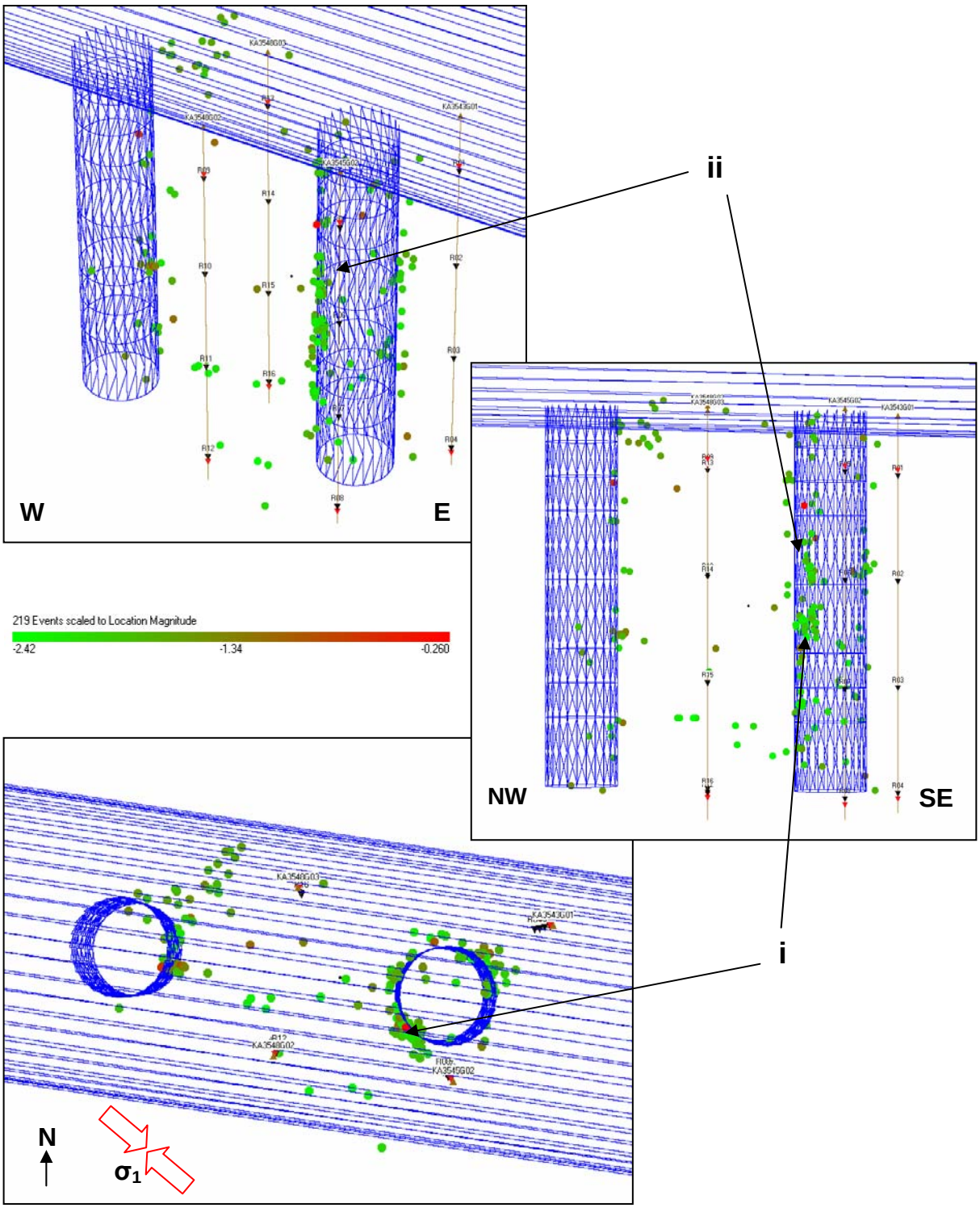

Figure 5-19: *Three views of AE activity located around deposition holes DA3545G01 and DA3551G01. (Top: Oblique view looking North. Middle: Transverse view looking north. Bottom: Plan view). Two clusters are marked i and ii.*

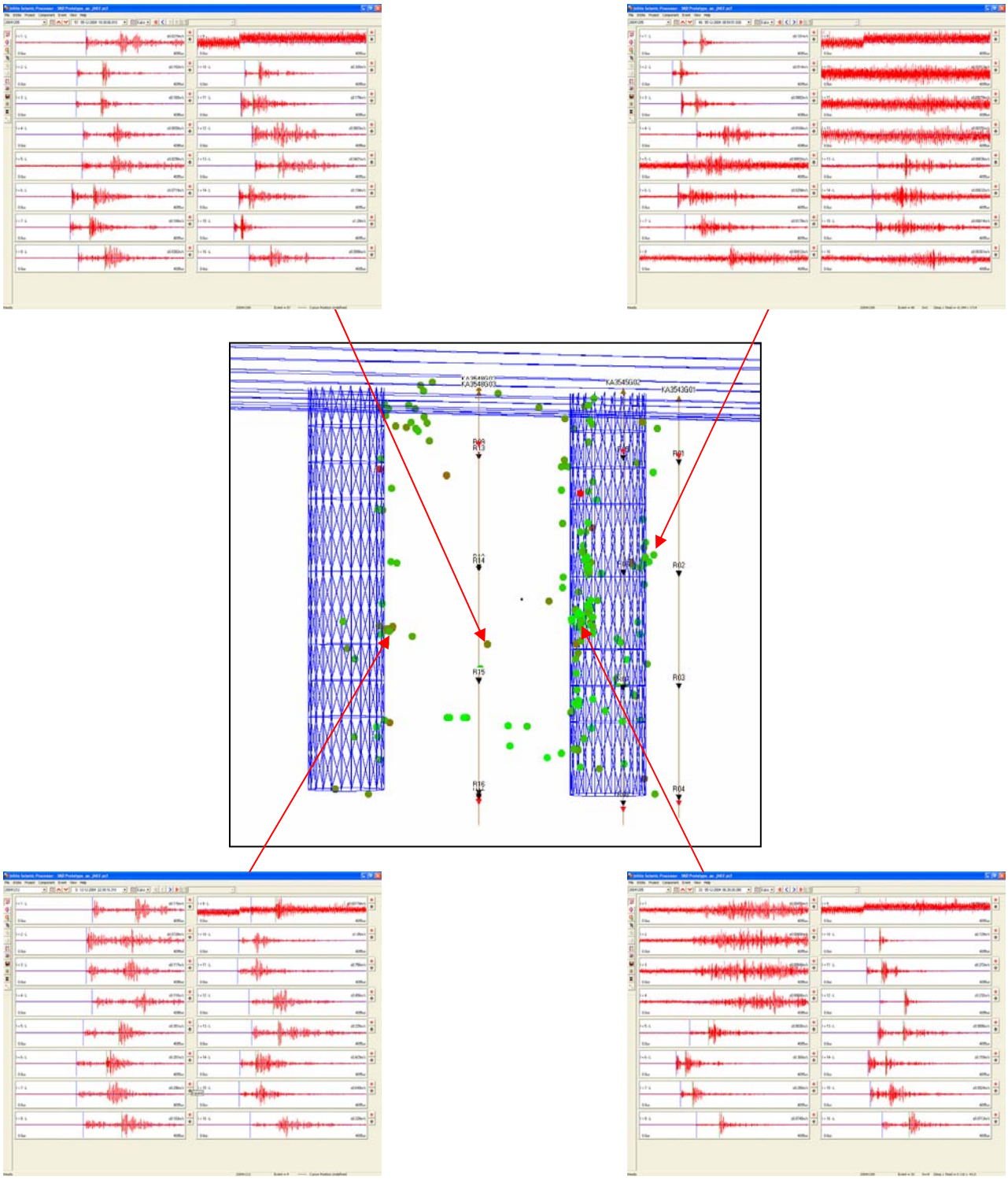

Figure 5-20: *Waveforms of selected events shown in relation to a transverse view of AE activity.*

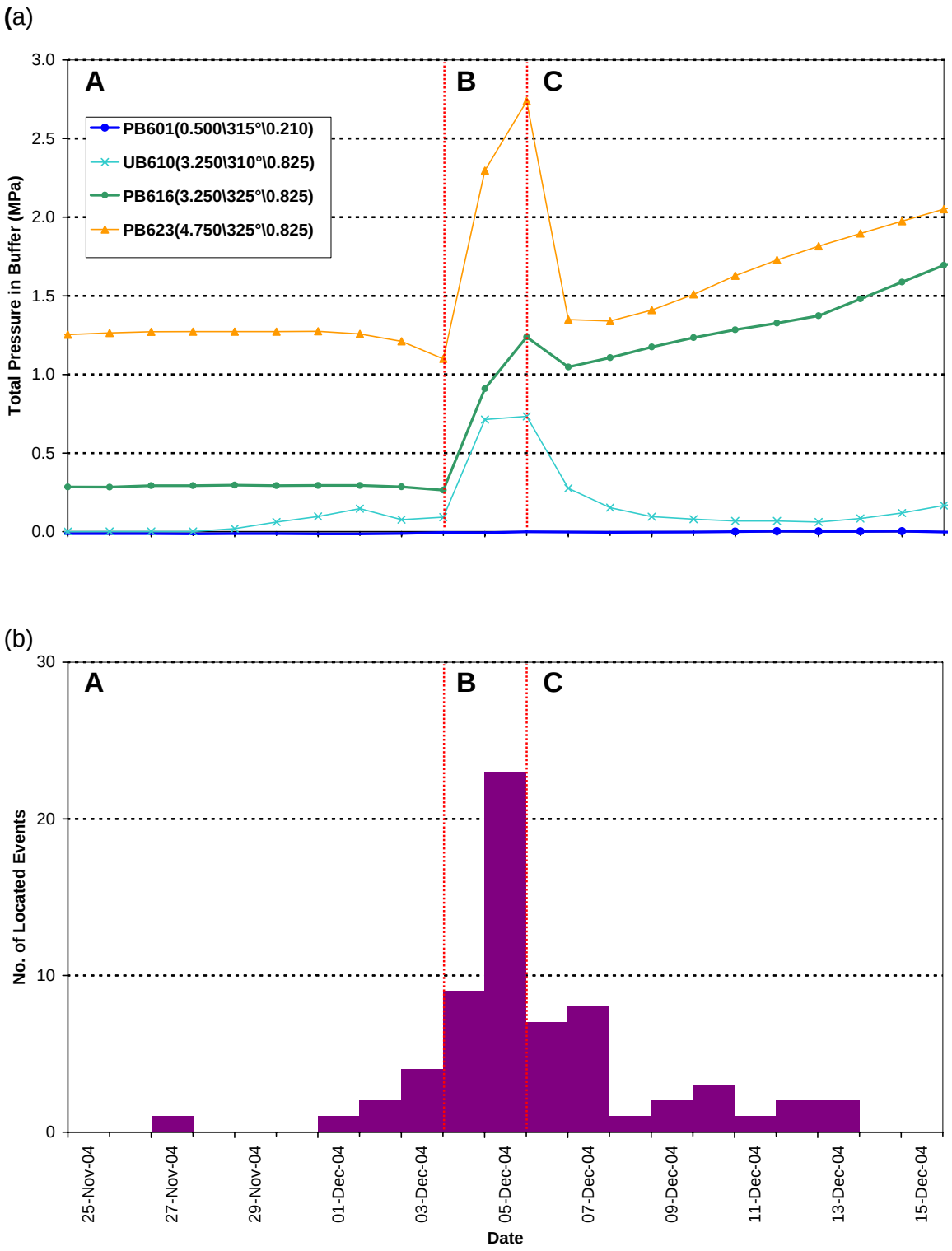

Figure 5-21: *Graphs showing how (a) pressure change in the buffer is related to (b) the number of located AEs. Regions A, B, and C are used in the*

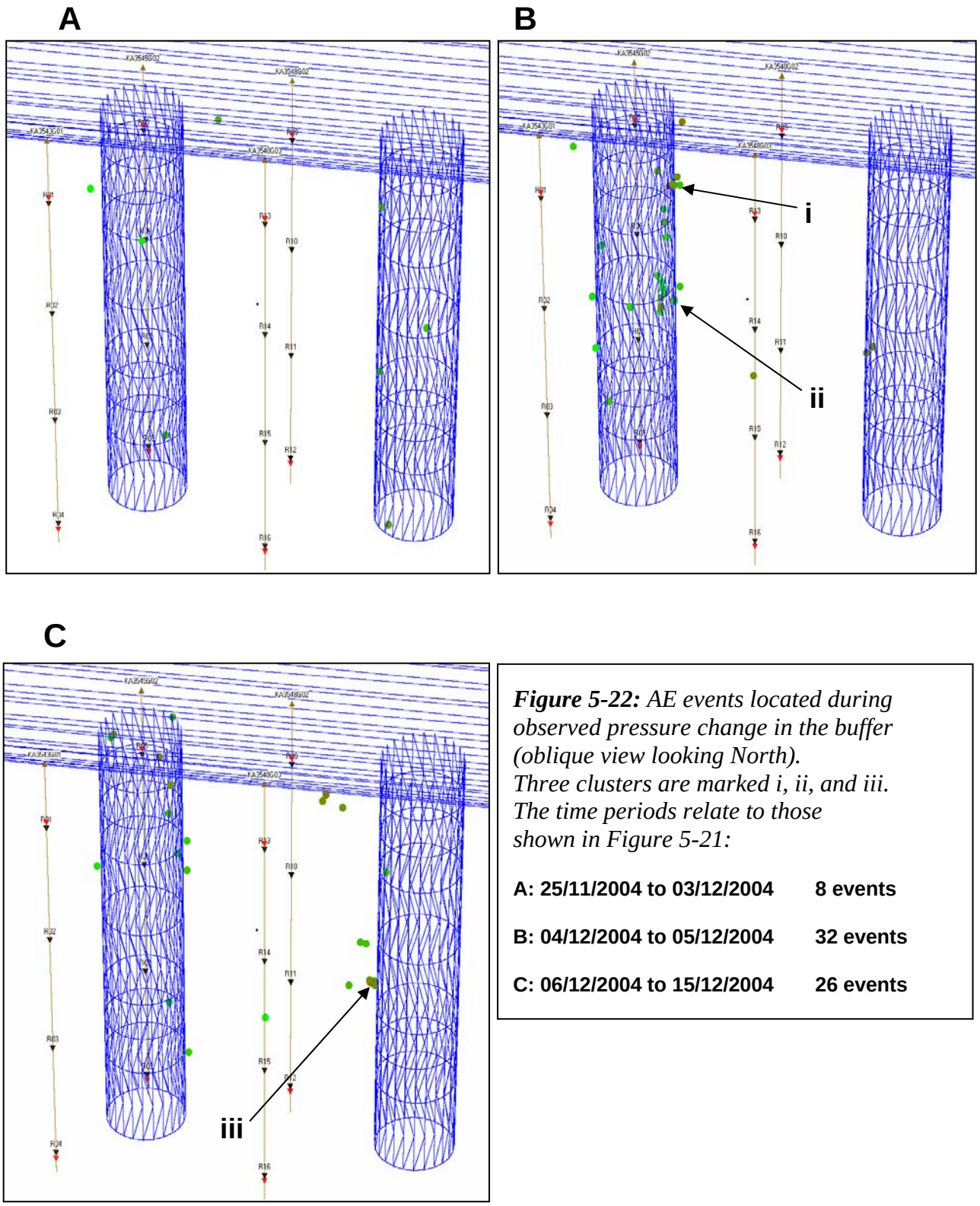

Figure 5-22: *AE events located during observed pressure change in the buffer (oblique view looking North). Three clusters are marked i, ii, and iii. The time periods relate to those shown in Figure 5-21:*

A: 25/11/2004 to 03/12/2004 8 events

B: 04/12/2004 to 05/12/2004 32 events

C: 06/12/2004 to 15/12/2004 26 events

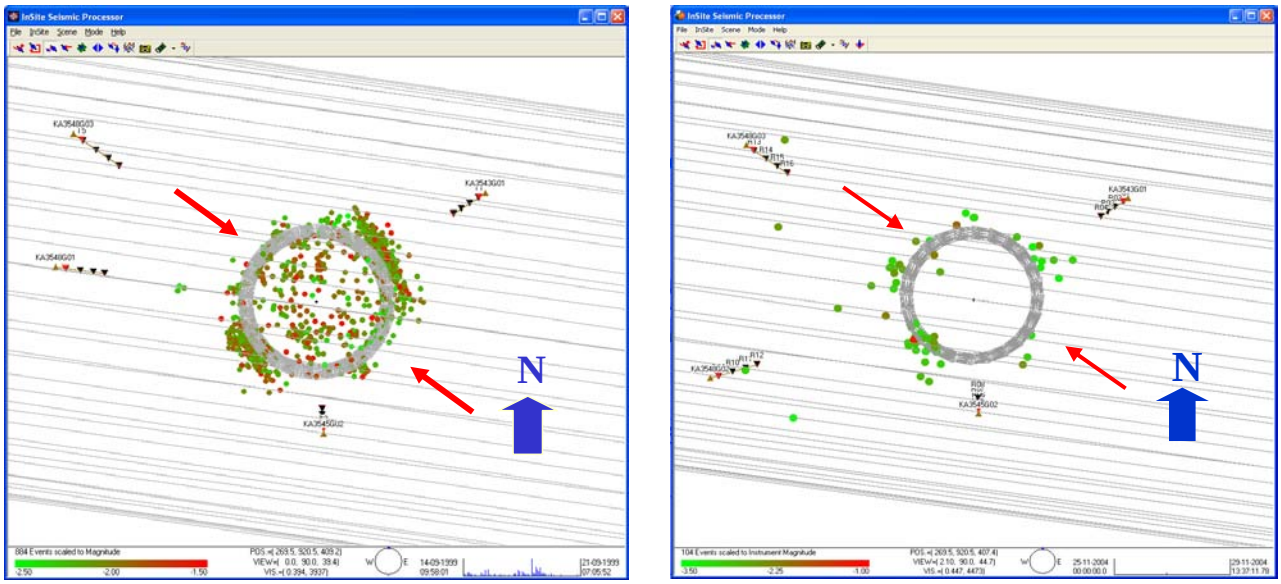

Figure 5-23: *Plan view of AEs located around deposition hole DA3545G01 during (a) the excavation phase, and (b) this reporting period. The red arrows mark the orientation of the principle stress.*

6 Results Summary and Conclusions

This report describes results from acoustic emission (AE) and ultrasonic monitoring around a canister deposition hole (DA3545G01) during the heating phase in the Prototype Repository Experiment at SKB's Hard Rock Laboratory (HRL), Sweden. This monitoring aims to examine changes in the rock mass caused by an experimental repository environment, in particular due to thermal stresses induced from canister heating and pore pressures induced from tunnel sealing.

Two different techniques have been used in this study to examine the rock mass. AE monitoring is a 'passive' technique similar to earthquake monitoring but on a much smaller distance scale (source dimensions of millimetres). AEs occur on microfractures in the rock mass when they are created or when they move. The data acquisition system triggers on AEs when they occur and records full-waveform information that is then processed to delineate the spatial and temporal distribution of the micro-fracture disturbance. Ultrasonic surveys are used to 'actively' examine the rock. In this case an array of transmitters sends signals to an array of receivers installed in the rock mass around the deposition hole during a daily survey. Amplitude and velocity changes on the ray paths, calculated using a cross-correlation technique, have then been used to examine changes in the material properties of the rock.

A permanent ultrasonic array, with transducers grouted into instrumentation boreholes, was installed in the rock mass in June 2002. Ultrasonic monitoring has been conducted in two periods between 20th March and 9th October 2003, and 29th September 2004 to 31st March 2005. The gap in monitoring occurred when the ultrasonic acquisition system was used for another experiment in the HRL (Pillar Stability Experiment). Results are presented here for the period between March 2003 and March 2005. Measurements from temperature and pressure instruments located in and around the deposition hole, provide an indication of the major environmental changes occurring during this period. In April 2003 temperature starts to increase after heaters are switched on. The rate of temperature increase is high over the first few months but reduces over time. By the end of the second monitoring period the maximum temperature measured on the deposition hole wall is 52.8°C. On 1st November 2004, drainage from the tunnel was closed resulting in a steady increase in total pressure (sum of bentonite swelling pressure and pore pressure) recorded in the tunnel backfill above the deposition hole. No increases in total pressure are observed for instruments on the side wall of the deposition hole until a rapid increase starting 4th December 2004.

The average P-wave velocity measured on the ultrasonic surveys at the start of heating is 5909m.s^{-1} and the average S-wave velocity is 3315m.s^{-1}. Towards the end of the monitoring period these velocities have risen to 5974 m.s^{-1} and 3343m.s^{-1} respectively. Large increases in measured signal amplitudes are observed at the end of November 2004 corresponding to an increase in signal quality at this time. Results from the ultrasonic surveys are presented in two phases corresponding to the first 6-month period, when thermal gradients were at their highest, and then the last 6 months when temperatures have reached a more steady state, but there are rapid and significant temporal changes in pressure.

The majority of processed raypaths during the heating period show consistent behaviour, with the general trend being an increase in signal velocities and amplitudes for both P- and S-waves. Young's Modulus, Poisson's Ratio, Crack Density and Saturation parameters have been determined from the P- and S-wave velocities. An increase in Young's Modulus occurs during the heating period (indicating the rock gets gradually stiffer) and Crack Density reduces. Heating applies a thermal stress to the rock mass around the deposition hole which interferes with the stress regime induced by the *in situ* stresses acting on the deposition hole void (as modelled by *Pettitt et al.*[2000]). The increase in observed velocity and amplitude values is due to closure of microcracks and pore spaces in the excavation damaged zone and surrounding stress-disturbed volumes indicating that the thermal stresses are acting to increase the compressive stresses around the deposition hole. When unconfined rock samples are heated in a laboratory environment thermal expansion of the sample causes tensile stresses leading to an opening of existing microcracks. In the case of the Prototype Repository, the rock around the deposition hole is confined by the *in situ* stresses and the bentonite buffer filling the tunnel and deposition hole. Expansion of the rock fabric cannot therefore act outwards and can only lead to compressive stresses acting on the existing microfractures and pore spaces. A minority of raypaths exhibit higher complexity and sometimes decreases in velocity. This may be due to the orientation and depth of the raypaths with respect to the different stress-disturbed, damaged regions or macroscopic fractures through which the ray paths travel. This response could be investigated further through the examination of thermal numerical models and laboratory experiments on confined rock samples.

The ultrasonic array geometry has been designed with 'skimming' raypaths that pass within a few centimetres of the deposition-hole void so as to sample the rock immediately adjacent to the deposition-hole wall. Raypaths have been categorised into six paths depending on the rock volume through which they sample. Skimming ray paths that pass through a region of low compressive, or tensile stress, induced around the void show increases in P-wave velocity (up to $40 m.s^{-1}$) which coincide with the start of heating and which then follow the trend in temperature change. Skimming raypaths that pass through a region of high compressive stresses, and permanent damage close to the tunnel wall (observed by relatively high AE activity during excavation), show a smaller average increase in P-wave velocity over the heating period with a drop in velocity imaged during the first few months. Average S-wave velocities on all raypath categories show a very similar pattern of increase except that raypaths passing through the low-compressive zone respond to heating much quicker. The initial drop in P-wave velocity is not observed on the S-waves. S-wave velocities do not respond to fluids so it can be inferred that the fall in P-wave velocities for ray paths passing through compressive zones is due to a de-saturation of the rock mass. P- and S-wave amplitudes all show very similar patterns of increase over time although there is some variation in the magnitudes of change overall. S-wave amplitudes generally show the larger increases.

The ultrasonic measurements show that the low-compressive stress, or tensile, region induced by the *in situ* stress field around the excavation void is more responsive to heating, exhibiting rapid increases in P- and S-wave velocity. The compressive zone responds similarly over the whole monitoring period, exhibiting increases in velocity, but both P and S-wave velocities respond slower in the first few months of heating. The difference in the rate of response between the two raypath categories is interpreted as a different magnitude of response of the microfractures in the rock mass to increasing thermal stresses. In the low-compressive region, existing microfractures will initially be

unloaded and hence more open than similar microfractures in the compressive region, where stresses act to clamp the fractures (i.e. the absolute Crack Density will be less). As thermal stresses are applied to the rock mass the open fractures will be far more sensitive to the stress increase and hence respond to a far greater extent, and far quicker, than those that are pre-clamped, resulting in more responsive ultrasonic signals. The compressive stresses will be variable with orientation and hence may explain small differences recorded on individual ray paths.

Another effect is superimposed onto the rock's response to thermal stresses. This is measured as a reduction in P-wave velocities compared to S-wave velocities in the first few months of heating. 'Saturation' values calculated from the measured P- and S-wave velocities show that a de-saturation occurs on all raypath categories during the first few months of monitoring, except for ray paths that pass through the low-compressive, or tensile, region. This must be caused by a drying of the rock mass as heat is applied to the rock (both pressure and temperature are acting to expel moisture). In the low-compressive, or tensile, region saturation increases during this period. This is probably caused by hot fluids expanding into the open microfracture fabric.

After closure of drainage in early November 2004, total pressure measurements show that pressure in the tunnel backfill above the deposition hole built up slowly, whereas pressure increases in the buffer inside the deposition hole occurred over a relatively short period of time (a few days). The highest magnitude changes in pressure inside the deposition hole occur nearest to the tunnel and they all occur at the same time (4^{th} to 5^{th} December). An interpretation of this response is that some form of event occurred on this date that suddenly allowed a transfer of pressure into the deposition hole from above. This interpretation is also borne out by observations that the canister itself is now damaged and by acoustic emission observations described below. The rapid increase in pressure resulted in significant changes to the character of many recorded waveforms from the ultrasonic surveys. This suggests that as pressure is increased in the rock surrounding the deposition hole, attenuation of the ultrasonic waves is reduced meaning that they can pass more efficiently through the rock medium. The reduction in attenuation is either a result of an increase in saturation in the rock mass (fluids are pushed into microcracks and pore spaces), or a result of a reduction in crack density caused by a closing of pre-existing microcracks, or a combination of the two. Significantly, velocity and amplitude changes recorded on the ultrasonic surveys occured up to 10 days *before* the pressure change is recorded inside the deposition hole.

A correlation is observed between the date on which the rapid changes in velocity and amplitude occur and the distance of the ray paths away from the tunnel, further down the deposition hole. The changes are observed between 26^{th} November and 1^{st} December and on all ray path categories irrespective of how close they pass the deposition hole void. This pattern does not appear in the pressure measurements recorded within the deposition hole on 4^{th}-5^{th} December. The modulus results show that the rock around the deposition hole generally stiffens and the crack density reduces prior to the recorded increase in pressure. Our interpretation of these results is that a pressure and/or fluid field migrated through the rock mass, initiated by pressure within the tunnel reaching a critical value on 26^{th} November (approximately 0.75MPa). A fluid 'front' may have used the existing macro-fracture network to propagate away from the tunnel. The pressure or fluid field reached the floor level of the deposition hole on 1^{st} December, but did not ingress into the deposition hole itself sufficiently to cause a response on the instruments contained there until 4^{th}-5^{th} December when a relatively sudden event occurred; it may have been

inhibited by the bentonite buffer material. The event may have been induced by a combination of the pressure increases around the deposition hole and a rapidly cooling canister (the heaters were switched off on 2nd December).

Processing of acoustic emissions (AEs) has resulted in 219 events located with high confidence during the whole reporting period. The events have been manually inspected to determine those that are real from human 'noise'. 73% of the events are located around the walls of deposition hole DA3545G01 within the volume of the array. The majority of these locate close to the deposition hole wall, within the first 20cm. In plan the majority of events are distributed in the NE and SW quadrants and coincide with regions of increased compressive stress induced by the interaction of the stress field with the excavation void. This activity is interpreted as stress disturbance of the rock mass, particularly around pre-existing macrofractures that commonly intersect the excavation, or microcracking in the immediate vicinity of the fractures. 22% of the events are also observed around the neighbouring deposition hole (DA3551G01) and in the floor of the tunnel in volumes outside of the ultrasonic array. The remaining 5% locate within the pillar volume and all occur at a similar depth below the tunnel. They define an approximately horizontal planar feature. This level coincides with a semi-horizontal macroscopic fracture that is observed to intersect the deposition holes at this height.

The peak rate of observed AE activity coincides with the rapid changes in pressure in the Prototype. On 4th-5th December 2004 there is a rapid increase in total pressure recorded in the buffer inside the deposition hole. This is 35 days after drainage was switched off and coincides with damage to the canister. A peak of 32 events occurs on 5th December 2005, when pressure in the buffer is highest, predominantly locating around deposition hole DA3545G01. The increase in activity is therefore likely to be the result of stress changes in the rock around the deposition hole associated with this relatively sudden increase in pressure. The stress changes are inducing small scale movements on pre-existing microfractures created during excavation, or are inducing new microfractures in weaker volumes of the rock. Pore pressure increases may also assist in inducing slip on pre-existing microfractures, by reducing the normal stress on the fractures. The peak in activity is only over a short time frame of 2 days but acoustic emissions are still recorded 8 days after the peak in pressure, mainly locating on the pillar side of the neighbouring deposition hole (DA3551G01). These are likely to be created through the same mechanism.

The overall AE activity rate is low compared to excavation, which indicates that heating of the deposition hole canisters has not so far resulted in a significant creation of new micro-fractures or the disturbance of pre-existing fractures. It is concluded that the thermal-related activity is a re-initiation of the same stress-related processes that occurred during excavation, although with a much reduced intensity. The AE activity did not start immediately heating began suggesting that the thermal stresses had to reach a certain level before AEs were triggered. This is likely to be the result of the Kaiser effect (well documented in laboratory experiments) where the AE rate is zero, or close to the background level, so long as stress remains below the largest previously reached stress value. In this case the largest stress value is that induced immediately behind the advancing face of the deposition hole during its excavation. The monitoring has shown that the rock is sensitive to sudden changes in conditions in the deposition-hole environment, such as the increase in pore pressure when drainage from the tunnel was closed off. This change in environmental conditions created a disturbance in the stress field around the deposition hole that was sufficient to cause a disturbance to the rock mass and was detected in both the ultrasonic survey and AE results.

References

Andersson, J.C., *Äspö Pillar Stability Experiment: Feasibility Study*, International Progress Report IPR-03-01, Swedish Nuclear Fuel and Waste Management Company, Sweden, 2002.

Collins, D.S. and R.P. Young, 2003. OMNIBUS Hardware Development in Months 19-24, Liverpool University, *in OMNIBUS Year 2 Progress Report*.

Baker, C., J. Hazzard, and R.P. Young. A three dimensional discontinuum model of the excavation of a deposition hole at the Äspö HRL. Äspö Hard Rock Laboratory International Technical Document ITD-00-15, Swedish Nuclear Fuel and Waste Management Company, Sweden, 1999.

Goudarzi, R. and L-E. Johannesson, 2004. *Sensor Data Report (Period: 010917-040901). Prototype Repository. Report No: 11*, Swedish Nuclear Fuel and Waste Management Company, Sweden, 2002.

Haycox, J.R., W.S. Pettitt, and R.P. Young, 2004. *Acoustic Emission and Ultrasonic Monitoring of the Äspö Pillar Stability Experiment*. ASC report to Swedish Nuclear Fuel and Waste Management Company, Sweden.

Johannesson, L-E., 2005. *Pers. comm.*

Lavrov, A., The Kaiser effect in rock: principles and stress estimation techniques, *International Journal of Rock Mechanics & Mining Sciences*, 40, 151-171, 2003.

Leijon, B., *Summary of Rock Stress Data from Äspö*, Äspö Hard Rock Laboratory Progress Report 25-95-15, Swedish Nuclear Fuel and Waste Management Company, Sweden, 1995.

Maxwell, S.C., and R.P. Young, A controlled in-situ investigation of the relationship between stress, velocity and induced seismicity, *Geophys. Res. Lett., 22*, 1049-1052, 1995.

Patel, S., L.-O. Dahlstrom, and L. Stenberg, *Characterisation of the Rock Mass in the Prototype Repository at Äspö HRL Stage 1*, Äspö Hard Rock Laboratory Progress Report HRL-97-24, Swedish Nuclear Fuel and Waste Management Company, Sweden, 1997.

Pettitt, W.S., C. Baker, and R.P. Young, *Acoustic emission and ultrasonic monitoring during the excavation of deposition holes in the Prototype Repository*, International Progress Report IPR-01-01, Äspö Hard Rock Laboratory, Swedish Nuclear Fuel and Waste Management Company, Sweden, 1999a.

Pettitt, W.S., C. Baker, and R.P. Young, *Acoustic emission and ultrasonic monitoring during the excavation of deposition holes in the Canister Retrieval test*, International Progress Report IPR-01-02, Äspö Hard Rock Laboratory, Swedish Nuclear Fuel and Waste Management Company, Sweden, 1999b.

Pettitt, W.S., C. Baker, and R.P. Young, *Analysis of the in-situ principal stress field at the HRL using acoustic emission data*, International Progress Report IPR-01-09, Äspö Hard Rock Laboratory, Swedish Nuclear Fuel and Waste Management Company, Sweden, 2000.

Pettitt, W.S., C. Baker, R.P. Young, L. Dahlstrom, and G. Ramqvist, The assessment of Damage Around Critical Engineering Structures Using Induced Seismicity and Ultrasonic Techniques, *Pure and Applied Geophysics*, **159**, 179-195, 2002.

Pettitt, W.S., Baker, C., Collins, D.S., and R.P. Young, 2005. *InSite Seismic Processor – User Operations Manual Version 2.12*. Applied Seismology Consultants Ltd., Shrewsbury, UK.

Pettitt, W.S. and J.R. Haycox, Acoustic emission and ultrasonic monitoring of deposition hole DA3545G01 during the excavation and heating phases. In *SAFETI Final Technical Report*, University of Liverpool, UK.

SKB, *Äspö Hard Rock Laboratory: Current Research Projects 1998*, Swedish Nuclear Fuel and Waste Management Company, Sweden, 1999.

Staub, I., J.C. Andersson and B. Magnor, *Äspö Pillar Stability Experiment: Geology and mechanical properties of the rock at TASQ*, Report R-04-01, Swedish Nuclear Fuel and Waste Management Company, Sweden, 2004.

Telford, W.M., Geldart, L.P., and Sheriff, R.E., *Applied Geophysics: Second Edition*, Cambridge University Press, 1990.

Young, R.P., C.D. Martin, R. Murdie, J. Alcott, S. Falls, I. Stimpson, and S. Yazici, *Numerical Modelling, Acoustic Emission and Velocity Studies of the Excavation Disturbed Zone at the Hard Rock Laboratory*, Äspö Hard Rock Laboratory Technical Note, Swedish Nuclear Fuel and Waste Management Company, Sweden, 1996.

Young, R.P. and W.S. Pettitt, Investigating the stability of engineered structures using acoustic validation of numerical models, in *Geotechnical Special Publication No 102*, edited by J.F. Labuz, S.D. Glaser, and E. Dawson, pp. 1-15, ASCE, USA, 2000.

Zimmerman, R.W and M.S. King, Propogation of acoustic waves through cracked rock, *20th Symposium on Rock Mechanics*, Rapid City, SD, 1985.

Appendix I Processing Parameters

Ultrasonic survey processing parameters:

PROCCESSING PARAMETERS **Velocity survey processing**

EVENT INITIALISATION	
View/process waveforms by	Channel
Channel-view Width-to-height ratio	6
Waveform Response type	Set from sensor
Sampling time	1
Time units	Microseconds
Pre-signal points	200
Spline sampling time	0.2
Waveform To point	1023
P-Time correction	0
S-Time correction	0
Automatically update Channel Settings	NOT SET
Project Files	NULL

AUTO PICKING	
Allow P-wave-autopicking	YES, Use first peak in the auto-pick function
Back-window length	100
Front-window length	35
Picking Threshold	4
Min. Peak-to-Peak amplitude	0
Allow S-Wave Autopicking	YES, Use first peak in the auto-pick function
Back-window length	100
Front-window length	35
Picking Threshold	5
Min. Peak-to-Peak amplitude	0
Allow Automatic Amplitude Picking	YES
Use Velocity Window Picking	YES
P-wave Min. Velocity/Max. Velocity	4500, 6500
S-wave Min. Velocity/Max. Velocity	2500, 3500

CROSS-CORRELATION	
CCR Events	Referenced to a Survey
Reference Component	All Data “20041208005920” Heating “20030320150034” Pressure Change “20041208005920”
Reference Event	NULL
Window construction method	Front to Back
Window comparison method	Fixed to reference picks
Window Parameters	Back-window length = 20 Front-window length=30 Rise-time multiplier = NULL Power to raise waveform =1 Split to a Spline function = YES Obtain absolute waveform= NOT SET

LOCATER	***(not used in velocity surveys)***
Method	SIMPLEX INTO GEIGER
Method settings Simplex settings Geiger settings	Tolerence = 0.01 LPNorm = 1 P-wave weighting = 1 S-wave weighting = 1 Use Outlier Identification = NOT SET Arrival error factor = ×2 Tolerence (Loc. units) = 0.01 Step size (Loc.units) = 0.1 Max. Iterations = 100 Conditional No. Limit = 10000000000
Velocity Structure	Homogeneous Isotropic
Velocity Structure settings	P-wave velocity = 5973.85 m/s S-wave velocity = 3342.705 m/s Attenuation = 200 Q(S) value = 100
Data to use	P-wave Arrivals Only
Distance units	Metres
Wotrking time units	Microseconds
Min P-wave arrivals	0
Min S-wave arrivals	0
Min Independent arrivals	5
Max. Residual	20
Start point	Sart at the centroid of the array
Write report to RPT	NOT SET
Source parameters	Set to calculate automatically

AE processing parameters:

PROCCESSING PARAMETERS **AE processing**

EVENT INITIALISATION	
View/process waveforms by	Channel
Channel-view Width-to-height ratio	6
Waveform Response type	Set from sensor
Sampling time	1
Time units	Microseconds
Pre-signal points	200
Spline sampling time	0.2
Waveform To point	1023
P-Time correction	0
S-Time correction	0
Automatically update Channel Settings	SET
Project Files	NULL

AUTO PICKING	
Allow P-wave-autopicking	YES, Use max peak in the auto-pick function
Back-window length	100
Front-window length	35
Picking Threshold	5
Min. Peak-to-Peak amplitude	0
Allow S-Wave Autopicking	YES, Use max peak in the auto-pick function
Back-window length	100
Front-window length	35
Picking Threshold	5
Min. Peak-to-Peak amplitude	0
Allow Automatic Amplitude Picking	NOT SET
Use Velocity Window Picking	YES
P-wave Min. Velocity/Max. Velocity	4500, 6500
S-wave Min. Velocity/Max. Velocity	2500, 3500

CROSS-CORRELATION	***(not used in AE prossessing)***
CCR Events	NOT SET
Reference Component	NOT SET
Reference Event	NULL (not activated)
Window construction method	Individual
Window comparison method	Fixed to reference picks
Window Parameters	Back-window length = 31 Front-window length = 31 Rise-time multiplier = NULL Power to raise waveform =1 Split to a Spline function = NOT SET Obtain absolute waveform= NOT SET

LOCATER	
Method	SIMPLEX INTO GEIGER
Method settings Simplex settings Geiger settings	Tolerence = 0.01 LPNorm = 1 P-wave weighting = 1 S-wave weighting = 1 Use Outlier Identification = NOT SET Arrival error factor = ×2 Tolerence (Loc. units) = 0.01 Step size (Loc.units) = 0.1 Max. Iterations = 100 Conditional No. Limit = 10000000000
Velocity Structure	Homogeneous Isotropic
Velocity Structure settings	P-wave velocity = 5973.85 m/s S-wave velocity = 3342.705 m/s Attenuation = 200 Q(S) value = 100
Data to use	P-wave Arrivals Only
Distance units	Metres
Working time units	Microseconds
Min P-wave arrivals	0
Min S-wave arrivals	0
Min Independent arrivals	5
Max. Residual	20
Start point	Sart at the centroid of the array
Write report to RPT	NOT SET
Source parameters	Set to calculate automatically

EVENT FILTER	
Date and Time	NOT SET
Location volume	Minimum = (235, 880, 420)
	Maximum = (300, 964, 463)
L. Magnitude	NOT SET
Location Error	1
Independent Instruments	Minimum = 0

SOURCE PARAMETERS	
Automatic source-parameter windows	P-wave back window = 10
	P-wave front window = 50
	S-wave back window = 10
	S-wave front window = 50
Source parameter calculations	Min number to use = 3
Automatic source-parameter windows	Apply Q correction = SET
	Source density = 2640
	Source shear modulus = 39131400000
	Av. radiation coefficient: Fp = 0.52 ,Fs = 0.63
Source parameter calculations	Source coefficient: kp = 2.01 , ks = 1.32
Magnitude calculations	Instrument magnitude = 1 * log (ppV) +0
	Moment magnitude = 0.666667 * log(Mo) + -6